UNIVERSITY OF CALIFORNIA
RIVERSIDE

Femtosecond Laser-Induced Oxide Formation on Molybdenum Thin Films in Varying Low-Pressure Oxygen Environments

A Thesis submitted in partial satisfaction
of the requirements for the degree of

Master of Science

in

Mechanical Engineering

by

Jon Andrew Redenius

June 2015

Thesis Committee:
Dr. Guillermo Aguilar, Chairperson
Dr. Santiago Camacho-Lopez
Dr. Javier E. Garay

The Thesis of Jon Andrew Redenius is approved:

Committee Chairperson

University of California, Riverside

Acknowledgements

This work was sponsored by scholarships from the University of California Institute for Mexico and the United States (UC MEXUS).

On a personal note, I would like to acknowledge Dr. Santiago Camacho-Lopez, Dr. Javier Garay, and Dr. Guillermo Aguilar for serving on my defense committee for this thesis. Additionally I thank Dr. Guillermo Aguilar for serving as my graduate advisor during my time at UC Riverside, for taking me into his lab and giving me the opportunity to learn and develop my thoughts, skills, and methodology in his optics lab. I appreciate all of your guidance.

I would also like to thank the several machinists involved with the work in this thesis. I would like to thank Stanley Sheldon in the UC-Riverside glass shop for creating and molding the quartz hemisphere for the pressure chamber. I would also like to thank Fabian Alonso Cordero from Centro de Investigacion Cientifica y de Educacion Superior de Ensenada (CICESE) for his expertise in SEM imaging and Israel Gradilla from Centro de Nanociencias y Nanotecnologia UNAM for his help with the FIB cuts.

Lastly, I would like to thank all my labmates past and present whom have helped me along the way these last two years; challenging me and supporting me. I thank you all for the fun and the companionship.

ABSTRACT OF THE THESIS

Femtosecond Laser-Induced Oxide Formation on Molybdenum Thin Films in Varying Low-Pressure Oxygen Environments

by

Jon Andrew Redenius

Master of Science, Graduate Program in Mechanical Engineering
University of California, Riverside, June 2015
Dr. Guillermo Aguilar, Chairperson

Pulsed laser processing is a technique to induce optical and structural changes in materials, such as oxide line and ring structures, when metallic samples are irradiated with high intensity lasers in oxygen and mixed atmospheres. The oxides, which can have very different electrical and optical properties, are gaining momentum in novel technical applications such as electrochromic devices, electrodes in microbatteries, gas sensors, and catalysts, among others. When a femtosecond laser irradiates a transition metal thin film, the thin film reacts with the gaseous species, producing different chemical and

structural phases, depending on the localized atmosphere and laser irradiance characteristics, e.g. the fluence, polarization, and duration of exposure. Here we present a processing study of femtosecond (fs) laser processing on molybdenum (Mo) thin films. The laser used is an Ytterbium-doped oscillator in the near infrared (1028 nm), ultrafast (230 fs pulse width), and with a high repetition rate (54 MHz). Irradiations are done under ambient air as well as pure oxygen gas conditions to document how the oxidations occur under varying environments. A custom-made, robust pressure enclosure was fabricated from scratch to be able to be mounted in an optical setup. Our results indicate that the high heating rates and electric-fields associated with laser processing allow the production of different phases and that a detailed fine-tuning of different variables can manipulate the oxidation of the samples. Raman spectroscopy, scanning electron microscopy, and atomic force microscopy are used in characterizing the oxidation of the different phases for the different irradiation parameters chosen. Our results indicate a high correlation between the increasing of the α-MoO3 formation area with the increasing of gas concentration and pressure.

Table of Contents

List of Figures

Chapter 1

Chapter 2

Chapter 3

Chapter 4

List of Tables

Chapter 1: Motivation and Introduction

1.1 Motivation

Numerous transition-metal oxides have begun to attract the consideration of engineers and scientists in the chemical, physical, and material science realm. One such transition metal in which the oxides are gaining extensive study is molybdenum. The dioxide, MoO_2 (molybdenum IV), and the trioxide, MoO_3 (molybdenum VI), are the two oxides of molybdenum that have various, investigated technical applications. Many deposition techniques have been used to form molybdenum and molybdenum oxide thin films, including Pulsed Laser Deposition [1], RF Magnetron sputtering [2,3], Chemical Vapor Deposition [4, 5], and wet chemistry methods [6]. It has been recently shown that in the low pulse energy, short pulse width regime that lasers can produce specific oxides when irradiated on a metallic thin film [7–9]. Laser processing is much cheaper and less invasive than any of the chemical procedures, so it should be explored as a clean and waste-less process.

The development and implementation of femtosecond lasers has opened up a new arena for novel technical applications; that of pulsed laser processing. Due to laser-material interactions at the femtosecond timescale, femtosecond lasers can precisely process metallic thin films and technical ceramics in innovative and original ways. In technical ceramics and other semiconductors, waveguides [10], microfluidics and

optofluidics [11] are among the major areas where femtosecond laser processing is prominent.

Laser-processable thin film oxides are being used in many different innovative technologies. Gesheva et al. [5] have studied molybdenum and tungsten oxide films for their electrochromatic tunability for a given electrical charge. Rouhani et al. [12,13] have begun study on which molybdenum ion and oxygen vacancies are responsible for the colorization and photochromism of MoO3 thin films. Heise et al. [14] have used picosecond lasers to be able to selectively structure the molybdenum electrodes currently used in CIS thin film solar cells. Molybdenum oxides are currently being looked into as electrodes in lithium-ion batteries. Lee et al. [4] have been working on methods to measure and improve the desirable long-term nanostructural order which effects the trioxides use as a reversible capacitor. Molybdenum oxides are their gas sensing properties are a big area when applications can be feasibly achieved. Yao et al. [15] showed gaschromic measurements and response of the α phase trioxide MoO3 when exposed to H2 gas. Sunu et al. [16] investigated the gas sensing properties of MoO3 in addition to the moisture-sensitive electrical conductivity. Ahire et al. [17] studied the possibility of high-working temperatures of MoO3 thin films as a sensor for different gases, concluding it's high sensing abilities as a hydrogen sulfide sensor.

Prior studies have shown that scans from a femtosecond laser on molybdenum thin films oxidize the local target area [7]. However, it has yet to be seen how different gaseous environments can affect the irradiations and resulting oxides based on varying

laser parameters. Preliminary studies showed considerable differences in the processing results when thin films were laser processed in varying gaseous atmospheres.

1.2 Pulsed Laser Processing

Pulsed laser processing has become more and more prevalent with the introduction and continued implementation of femtosecond lasers. Because femtosecond lasers are able to process materials without the formation of large heat-affected areas due to non-thermal processes, the use and precision of the laser processing has become a valuable tool in technological advancements. Novel areas of femtosecond laser processing include the induction of phase transformation, ablation, and patterning of many different metallic thin films and semiconductors. Advantages to the processing of metallic thin films by femtosecond lasers include the power requirements, rapid processing time, atmospheric requirements, and spatial resolution.

Femtosecond lasers, due to the repetition rate of the oscillator, can offer successful processing due to the sheer number of pulses hitting the target. This allows the power requirements to be lower than other gas and solid state lasers used in processing applications. The per-pulse energy of femtosecond lasers are on the order of nanojoules; in our specific case for out Mikan oscillator, the full-power, per-pulse energy is about 20nJ.

Even though the per-pulse energy is very low, femtosecond laser processing still has considerable processing uses due to the repetition rate of the pulses. Typical femtosecond lasers oscillate and deliver pulses in the MHz range. It is this high-volume

delivery of pulses that enable femtosecond lasers to process materials very quickly. The Mikan laser in the Optical Characterization Lab delivers pulses at 54 MHz; this means that in even in 1 millisecond, 54 thousand pulses have been delivered to the target. The ultrafast processing also does not allow the thin films to cool down at all between pulses.

Atmospheric requirements for pulsed laser processing are bare minimum – none. Pulsed laser processing of thin films can be done in room temperature and air, while still being able to obtain desired results in oxidation or ablation of the thin films. It is unknown whether or not adapting and varying the atmospheric conditions can elicit different properties or produce similar changes using lower powers; this is the purpose of the study. If altering the atmosphere and adding a pressurized gas can improve the tunability of laser processing, the precision and repeatability in obtaining the desired oxidation and ablation can be improved and optimized.

Femtosecond lasers, being an optical amplification device, can have manipulable optics as long as the setup is rated for the applicable laser wavelength. Being able to focus the outputted laser light is an important tool in obtaining a large power density due to the power-two relation based on irradiated area. Because of this, the energy density can easily approach the all-important boundary between oxidation and ablation of the thin film material. Using a combination of lenses, the laser beam waist can easily be reduced by up to two orders of magnitude, thereby increasing the energy deposited in a given area. It is this small scale spatial resolution that gives femtosecond laser processing

another desirable trait, to be able to focus the beam in a very small and precise area opens up many possible technological applications.

1.3 Thin Film Oxidation

True to most materials on earth, metallic thin films are subject to passivation. Passivation is the process in which metals form an oxide layer on their surface simply by being exposed to air. Passivation acts as a shield or barrier to prevent corrosion in a metal. The passive layer on thin films is normally several nanometers thick and generally not seen by advanced microscopy techniques. This passive oxide layer binds tightly in molybdenum thin films, thereby stopping the oxidation from penetrating deeper into the metal, acting as a defacto shield to prevent further oxidation [18].These passive layers can form on thin film surfaces within seconds of exposure to room temperature air [19].

Molybdenum is known for being able to volatize in relatively low temperatures and especially in atmospheric conditions [20]. To oxidize the molybdenum metal thin film, oxygen ions diffuse through the already-present passive oxide layer to react with the molybdenum atoms to form the new oxide layer [21]. The metal's molybdenum atoms are excited due to heating in the electronic regime from the femtosecond pulses [9]. This oxide layer is much more fused and deeper than the passive layer. This new oxidized molybdenum level is deep enough to be characterized by spectroscopic analysis. The new oxide layer composition depends on the oxygen ion concentration on the surface and the temperature reached during the femtosecond laser heating. This explains why the dioxide

(in molybdenum's case) is seen in irradiations before the trioxide, the diffusion energy required to form the trioxide is greater [9].

1.4 Molybdenum and its Oxides

Molybdenum is an earth transition metal that doesn't occur in nature as a free metal, but rather, in various compounds in minerals. Molybdenum is a fairly abundant metal, ranking 54th in world abundance [22]. Pure molybdenum is usually extracted from mined molybdenite and/or as a byproduct of copper mining. The United States is both the second highest producer of and storage country of molybdenum [22].

In particular, certain molybdenum oxides have been shown to have more potential use than others, though fabrication and synthesis techniques vary widely. Optical, chemical, electrical, and mechanical properties change based on fabrication technique, so some oxide may show more promise comparing methods of formation.

Molybdenum metal oxides are gaining use in catalyst applications [23,24], electrochromic devices [25], electrodes in microbatteries [24], and gas sensors [26].

Recently, the molybdenum trioxide has been being studied for use as a gas sensor after researchers noticed correlations between molybdenum and an already-in-use transition metal, tungsten [26,27]. US production of molybdenum is almost 8 times more than tungsten production [22], so it makes sense to seek more available metals for fabricating gas sensors. The conductivity of the molybdenum trioxide increases when

subjected to some form of nitrogen or carbon [3,26] and this change can quantitatively be measured. One drawback of the gas sensing use for these oxides is the decrease of performance in relatively low temperatures [16]; this can be attributed to how the thin film oxide was processed. Processing with ultrafast lasers is a still relatively new notion that needs to be explored, especially if the temperature performance range can be expanded. The laser in the Optical Characterization Laboratory is pertinent to this recently divulged method of oxidation. The laser and the relevant optics have been shown to be within the fluence range necessary to force oxidation. From brief initial experiments, the trioxide is the oxide formed around the immediate irradiation area. Knowing this, experimentation with the fluences required to potentially just obtain the trioxide can be done to obtain a desired growth.

Molybdenum thin films have been shown to ablate when irradiated with a femtosecond laser, so laser-assisted microdrilling remains an intriguing study to divulge into. Similar fluences to the MIKAN laser have microdrilled specific depths into molybdenum thin films within select regions. An issue in prior studies, though, is that a small amount of thin film residue stays within the ablation zone, altering the laser drilling mechanics and potentially increasing the thermally-affected zone [28].

Molybdenum thin films have been shown to change phase and composition when irradiated with short-pulsed, low energy lasers. Studies have been done that show different morphological phases occurring after molybdenum thin films are irradiated with femtosecond lasers at varying wavelengths and repetition rates. Only air-specific studies

have been documented; to the best of the author's knowledge and research, no prior insights have been done in any other pure or partial pressure gas conditions using low energy, femtosecond lasers. From these preceding studies, two primary oxides form from laser irradiation, MoO_2 and MoO_3.

1.5 Molybdenum Oxide Structure

MoO3 is classified as a metal-excess (n-type) semiconductor and MoO_2 is classified as an amphoteric electrical conductor. N-type oxides contain oxygen vacancies, so replacing the valent N_{3-} ions with divalent O_2- would increase oxygen vacancies which, in turn, increase the oxidation rate [29].

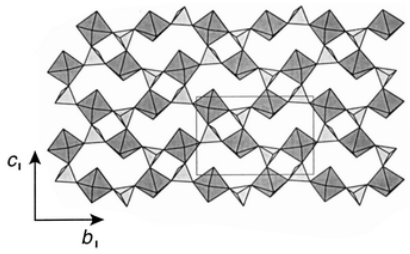

Figure 1.1: MoO_2 Structure [30]

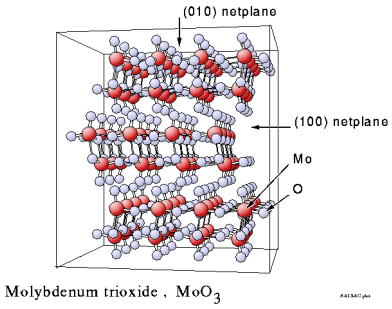

Figure 1.2: MoO_3 Structure [31]

The MoO_2 crystal structure is described as a distorted rutile tetragonal crystal structure. This is represented in Figure 1.1 [30]. The MoO_3 structure is composed of distorted octahedral layers in an orthorhombic orientation. This is represented in Figure 1.2 [31]. Both crystal structures are made up of MoO_6 octahedra.

1.6 Laser Heating

In femtosecond lasers, the processing of metal and metallic thin films still contain thermal heating due to the thermal diffusion time in metals still being in the picoseconds regime [11]. Because femtosecond lasers have pulses in the hundreds of femtoseconds, this minimizes the heat affected zone and optimizes the uses in micromaching. Femtosecond lasers actually reduce the thermal diffusion time in comparison to other lasers, so there is less of a heat affected zone and, consequently, higher precision in microfabrication results [11]. However, the initial reactions are actually due to the initial heating and moving of the electrons in the metal. These electrons then are able to transfer heat due to the equilibrium between the electron and the lattice via normal thermal diffusion [28].

The thermal heating due to a pulsed-laser has been researched and investigated recently [32]. Due to the high-repetition rate of the femtosecond laser in the Optical Characterization Lab, the laser can be modeled as a continuous laser if computing power is a limitation. If not, the laser heating equation, modified from the model derived by Bialkowski, is presented below in Equation 1.1.

$$T(r,t) = \frac{2\alpha Y_H E_0}{\pi \rho C_p w^2} * \sum_{m=0}^{M-1} \frac{1}{t_c + 2(t - mp)} * EXP\left(\frac{-2r^2}{w^2(t_c + 2(t - mp))}\right)$$

Equation 1.1 Femtosecond Laser Heating Equation

Where:

Y_h = Heat yield, material constant related to absorbed power

ρ = density, kg/m^3

t_c = characteristic mass diffusion time (equal to $w^2/4D$), s

D = diffusion constant, m^2/s

C_p = Specific Heat, J/K

E_0 = Energy per pulse, J

w = beam waist, m^2

α = attenuation coefficient, m^{-1}

t = time, s

m = current pulse number

p = pulse period (inverse of repetition rate), s

M = total number of pulses

The model assumes a semi-infinite material, which accounts for the lack of depth into the material in the equation. This equation models the two-dimensional (presented here in radial coordinates) outward temperature change and heat flux. It follows from the equation that the heat and temperature seen are dependent on material variables and that the absorption constant can greatly affect the resulting thermal heat transferred due to it directly affecting the characteristic time and thermal diffusivity.

1.7 Raman Spectroscopy and Methodology

An important tool to be able to characterize the irradiations is using Raman spectroscopy. The oxide rings and paths are in the micro-scale, so a characterization technique that can focus its beam onto small areas is paramount. The Raman spectrophotometer in the University of California, Riverside is owned and operated by the Analytical Chemistry Instrumentation Facility. The Raman microscope in the ACIF is a Horiba LabRAM HR, pictured in Figure 1.3, and has spatial resolutions in the 3 μm scale and spectral resolutions of around 1 cm^{-1} using the correct grating which enable its use in the oxide thin films studies.

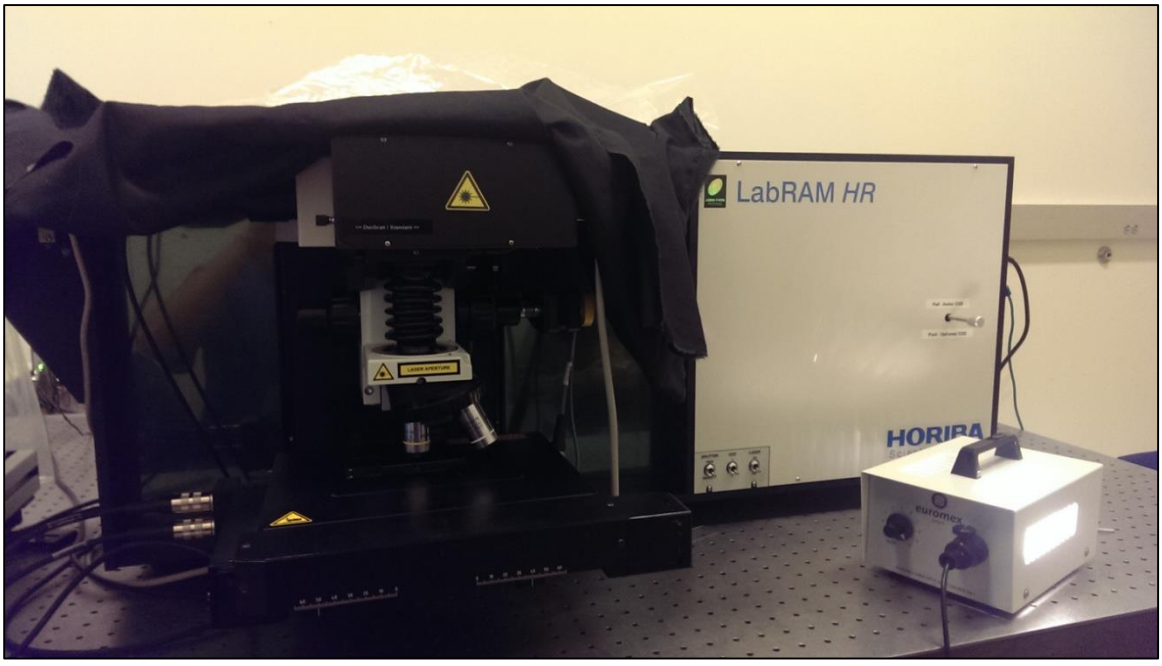

Figure 1.3: Horiba LabRAM HR Analytical Raman Microscope

The theory behind Raman spectroscopy involves the inelastic scattering of light (photon) particles. The incident laser in the Raman machine hits the sample target, and excitations and vibrations of the target molecules result. This transfers energy to and from the vibrating molecules. By scanning relevant ranges for a given material, a spectrum can be outputted in where a given intensity is plotted against the scanned wavenumbers. Wavenumber is a measurement of the spatial frequency of a wave, and can also be expressed in eVs. The vibrations and molecular excitations are unique for each material for a given wavenumber range. These plots can then be compared against reference plots and vibrational mode calculations in order to confirm and determine a sample's material makeup, in this case, the phase and oxide of the irradiated areas of the molybdenum thin films. Usually, metals aren't Raman active, but the metal oxides do show intense Raman bands, which allow us to use Raman spectroscopy in characterizing the oxidized thin film. The parameters used were 60 mW of emission power, 100 μm hole size, grating of 1800 gr/mm, and 3 passes of 45 second scans in the wavenumber range from 100 to 1100 cm^{-1}.

Chapter 2: Experimental Setup

2.1 Sample Preparation

The transition metal thin films used in this study were fabricated using Direct Current (DC) Magnetron Sputtering and were measured out to be 500 nm thick. DC Magnetron sputtering is a deposition technique in which a target is hit with ionized gas molecules that displaces atoms from the target's surface. These atoms then fly off and hit a substrate and bond at the atomic level. This creates a thin film of material that is uniform and very thin. In our case, the thin films were deposited on glass substrates. The process occurs under vacuum conditions in a chamber which is also pumped with argon gas in order to control the voltage hitting the material target. The DC Magnetrons allow specific configurations and timelines in the sputtering process in order to optimize for any given process. The different Magnetron settings allow for predictability and repeatability. The ionization of the gas accelerates the target atoms to the substrate on the other end of the chamber. The process is illustrated in Figure 2.1.

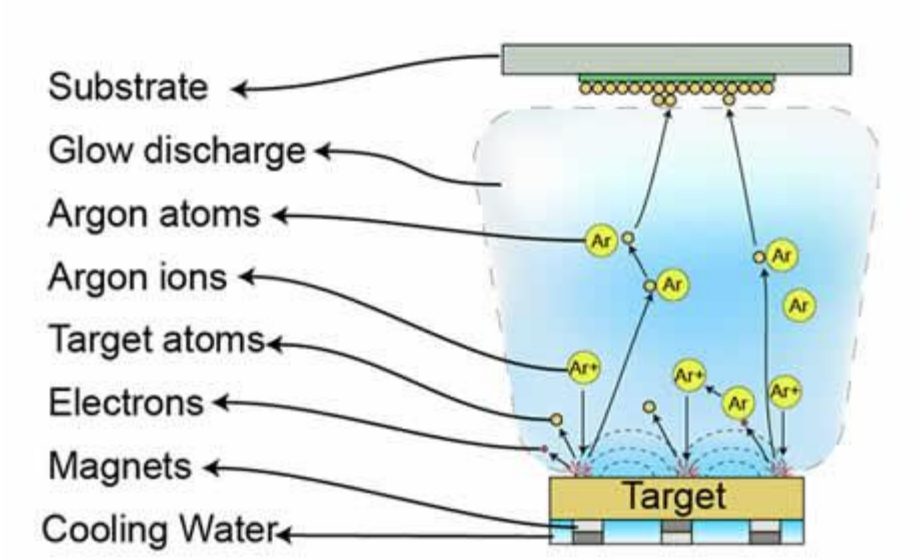

Figure 2. 1: DC Magnetron Sputtering Process [33]

Upon receiving the samples, they were cleaned using ultra-sonicating baths in both DI water and acetone. Before each irradiation, the samples were checked for homogeneity around the target area using a microscope and cleaned with methanol and acetone with light brushes using optical-rated tissues. The samples were then carefully placed on the target mounts with tweezers pinched at the ends and placed flat.

2.2 Confirmation of Homogeneity

Upon reception of the sputtered thin films, they were taken to Raman spectroscopy in order to confirm the molybdenum composition of the samples. The Raman spectra of the non-processed thin films are shown in Figure 2.2. This spectra is in line with the reported Raman spectra of bulk molybdenum [34].

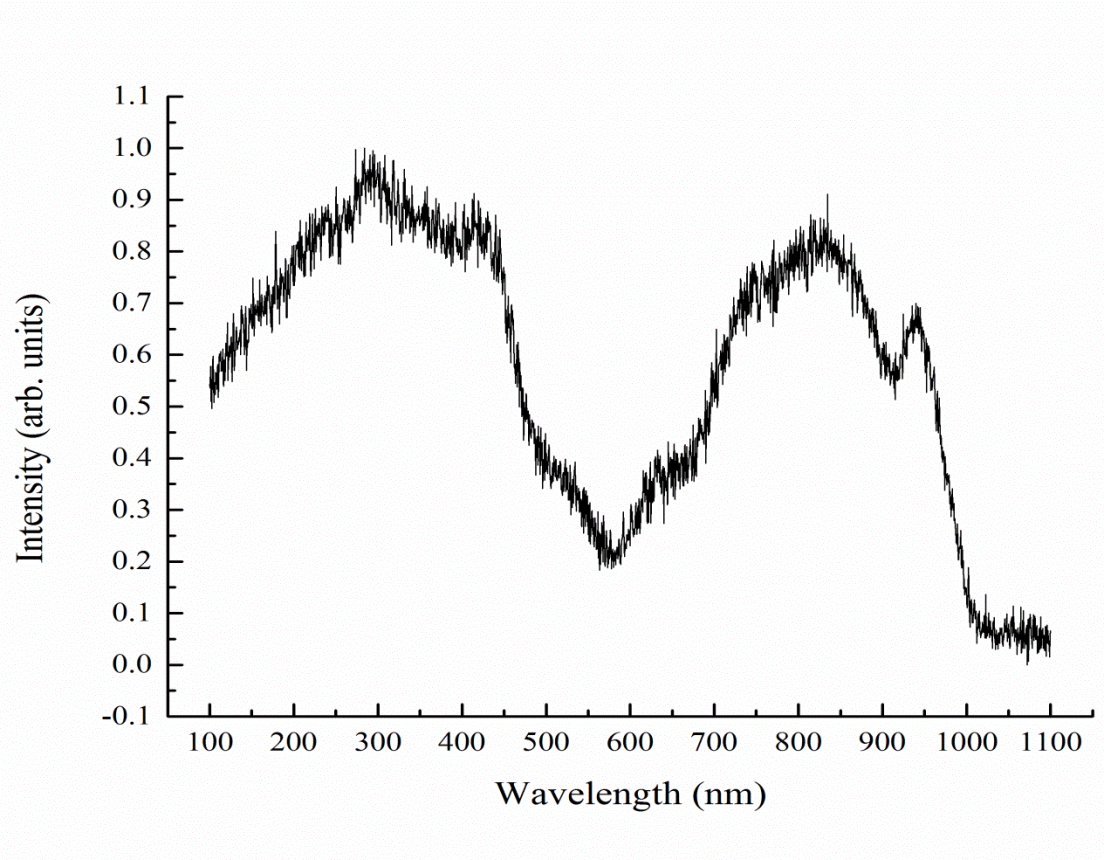

Figure 2. 2: Raman Spectra of un-irradiated molybdenum thin films

The samples were also checked under a microscope to ensure a homogenous and continuous thin film was deposited on the substrate without any contamination.

2.3 Experimental Setup

The experiments were conducted over a several month period in the Optical Characterization Lab in the Department of Mechanical Engineering, University of California – Riverside. The optical components were all mounted on an optical table. The

laser was an Amplitude Systèmes MIKAN oscillator with the properties tabulated in Table 2.1. The laser is pictured in Figure 2.3.

Type	Pulse Width (fs)	Repetition Rate (MHz)	Pulse Energy (nJ)	Max Power (mW)	Wavelength (nm)
Ti:sapphire	230	54	20	1080	1028

Table 2. 1: MIKAN Femtosecond laser properties

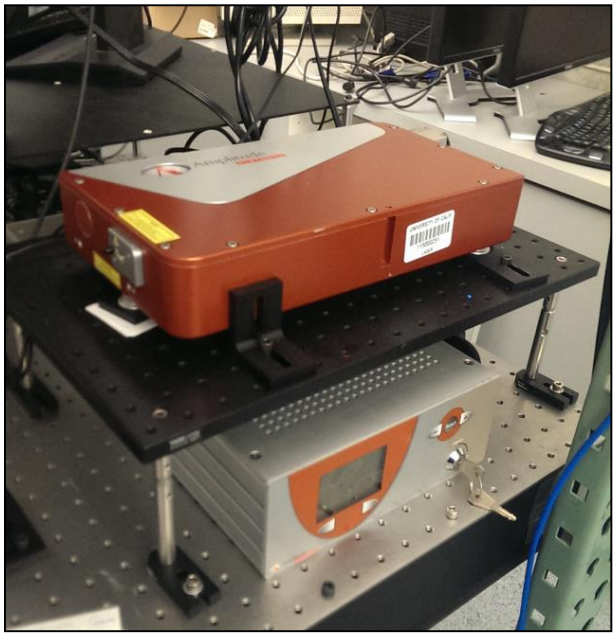

Figure 2. 3: MIKAN Femtosecond Oscillator

The MIKAN laser outputs a laser beam in the near infrared, at 1028 nm. This wavelength is invisible to the naked human eye so OD +5 level laser goggles are required to be kept on at all times while operating the laser. The beam was located and aligned with the aid of laser viewing cards, which utilize a photosensitive region that emits light

when a specific wavelength of laser light hits the card; in our case, in the near infrared. The laser emits, at full power, 1080 milliwatts. This then accounts for a pulse energy of 20 nanojoules due to the high repetition rate of the oscillator: 54 MHz. The pulse width of the laser is in the femtosecond regime, 230 fs. Femtosecond pulse width lasers are unique as the electron and thermal effects are mixed at this timescale; meaning there is no clear dominating physics in this regime and that both effects must be taken into account as a whole. This makes physical modeling the interactions in this time frame fairly difficult as the laser heating properties change based on the material being irradiated and its specific material and optical properties.

The laser outputs a Gaussian profile, and was slightly elliptical (~10%) upon being delivered to UC-Riverside. The diameter was approximately 4% greater in one direction, and the laser was specified to have an M^2 value of 1.06 and 1.04 for the two directions. The M^2 factor is a measure of beam quality of a laser; a perfect Gaussian beam has a value of 1. The beam diameter was measured at the $1/e^2$ value. The $1/e^2$ number is the width of the Gaussian profile at $1/e^2$ down from the maximum (~13.5%), this is a standard parameter used to quantify, determine, and compare beam width.

The laser was profiled several ways to confirm incident output beam size and shape. One strategy was to measure the beam spot using a CCD camera placed at 50 centimeters from the laser output. Neutral density filters needed to be used in order to preserve the sensor from damage due to the laser power. This Gaussian profile is shown in Figure 2.4. The Guassian function's analytical calculator in OriginPro 9 outputted a

151.02 pixel value for the FWHM. Using our CCD's pixel density of 7.6 um/pixel, this calculates to a 19.87 μm beam waist. A second method of cross checking the size of the laser was to compare the calculated incident laser beam waist on the sample with the size of the pocket or hole as measured on the microscope. Some thermal effects can be at play here that can change the shape of the path, but a clear, outlined, pattern and groove can be deciphered. This is shown and measured in Figure 2.5.

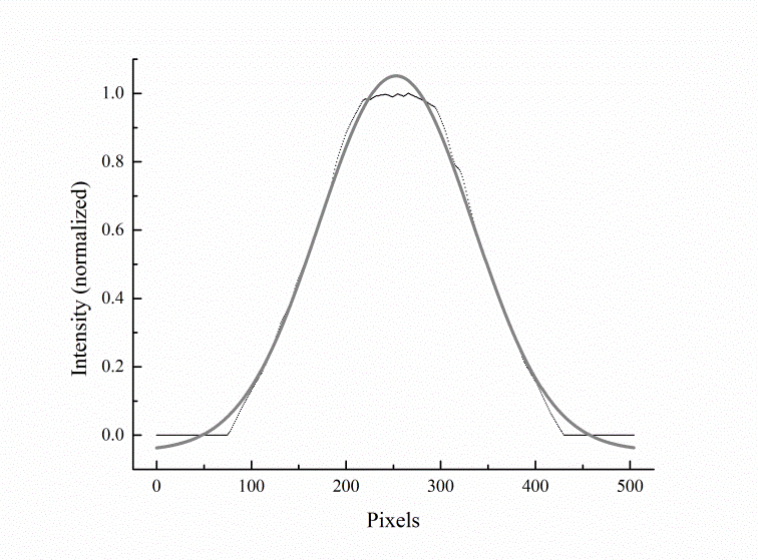

Figure 2. 4: Gaussian fit of laser beam waist

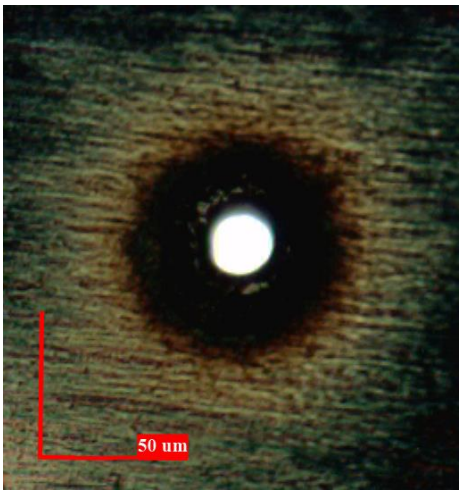

Figure 2. 5: Ablated hole of laser beam waist

At the laser beam exit are a wave plate and polarizer. The wave plate alters the phase of the polarization between the perpendicular components of the wave of light. The wave plate used in this experimental setup is the half-wave plate which polarizes the light linearly. The beam then enters a polarizer, which removes the unwanted polarization of the laser light. The wave plate-polarizer combination acts as an optical attenuator of the wave of light, allowing us to change the phase angle of the wave plate. This allows us to be able to have variable output power of the beam, which lets us achieve lower power densities than the specified, designed output.

The beam is then diverted off of a “P01” silver Thor Labs mirror which has high reflectivity for the NIR wavelengths. The beam then goes through an infrared-optimized beam splitter which routes the reflection back from the sample to the CCD camera. This is done to confirm the focus of the laser beam onto the sample, and can be removed once the most optimum focus is found to avoid the minimal power losses. The laser beam is

then focused onto the target using aspherical lens (Thorlabs, USA) of varying focal lengths in order to have control over the beam waist.

2.4 Pressure Chamber

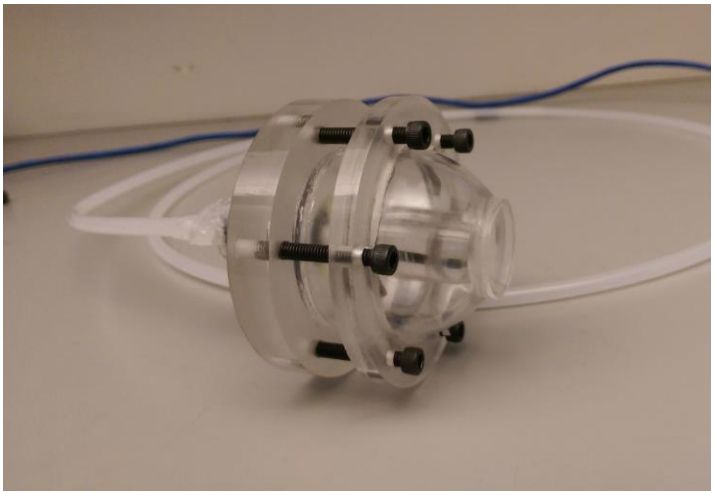

Figure 2. 6: Fully constructed pressure chamber with hose

To create atmospheric conditions for a specific gas, a robust enclosure was needed. The full enclosure-chamber is pictured in Figure 2.6. It was also required that whatever enclosure was designed needed to be predominantly optically transparent in the infrared regime to not have any power losses. After an exhaustive design process and material investigation, the most flexible design included using a quartz window with a flat incident exposure area with a domed curvature. This quartz window is shown in Figure 2.7. The quartz window was made with a lip around the outer diameter to have a plastic ring to be able to further screw and set the quartz sphere inside the plastic enclosure. The hemisphere and constraining rings are shown in Figure 2.8. The spherical

enclosure was then mounted onto a plastic backing which included the gas inlet and the varied target cylinders. The gas inlet, with a silicone sealant, are shown in Figure 2.9, along with the kinematic mount fitting groove. The cylinders were added to have flexibility on focusing the laser by being able to move the sample closer or further from the optical window.

Figure 2. 7: Spherical quartz window

Figure 2. 8: Quartz hemisphere with plastic latching ring and set screws

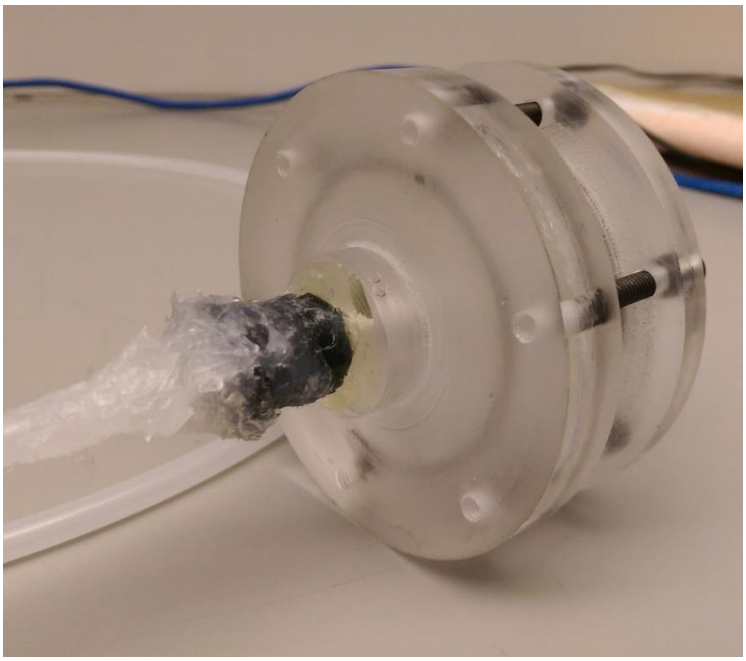

Figure 2. 9: Gas inlet and mount groove

The plastic mount was designed to be ultra-lightweight (~10 ounces) and fit into the kinematic mounts for precision alignment and focusing. The spherical enclosure was designed with a lip around the edge of a cylindrical portion in order to be fastened to the plastic mount. An O-ring on the enclosure-mount interface finalized the atmospheric seal. The lip and the fitted O-ring are shown in Figure 2.10.

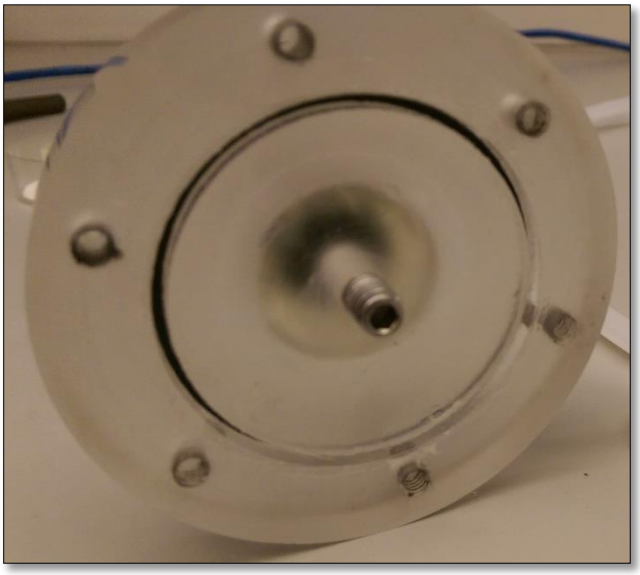

Figure 2. 10: Lip for quartz fitting with O-ring, included, the ¼-20 set screw

The acrylic mount was machined using a lathe to turn down the enclosure's kinematic mount fittings and CNC mills for the screw holes and O-ring groove. The plastic enclosure contains a tapped center in which the gas enters the chamber. The varied target mounts were then tapped with a ¼-20 thread and a set screw with a through hole was used to connect the mounts to the enclosure. The mounts were then cross-drilled for the gas to enter the chamber. One of the cross-drilled mounts is shown in Figure 2.11.

Figure 2. 11: Target cylinder with cross-drilled gas pathways

Figure 2. 12: Gas enclosure on kinematic optical mount

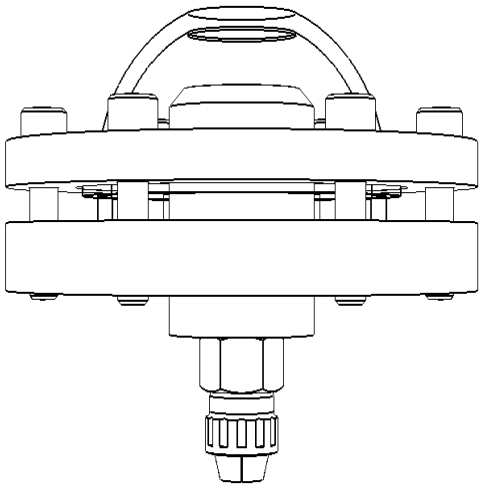

Figure 2. 13: Computer Aided Design sketch of gas enclosure

The complete enclosure and mount setup are pictured in Figure 2.12, with the quartz sphere. The Computer Aided Design sketch is show in Figure 2.13. The spherical quartz enclosure was made by the staff at the Glass Shop in the College of Natural and Agricultural Sciences at UC-Riverside. The plastic mount was fabricated in the Department of Mechanical Engineering Machine Shop at UC-Riverside by Optical Characterization Lab members. The gasses used were supplied by the Department of Mechanical Engineering at UC-Riverside, filled by Airgas. N_2 (Airgas, 99%), O_2 (Airgas, 99%), and Ar (Airgas, 99%) gases were used in the reported and prior studies. The gasses passed through a pressure meter to regulate the pressure of the chamber in an attempt to get vacuum conditions. The experiments were run under partial pressure conditions pulled by a diaphragm vacuum pump (Edwards, United Kingdom). These conditions were verified using a vacuum gage; measuring at 29 In-Hg (98% vacuum). A three-way valve was used in order to be able to pull vacuum and push gas via the same tube into the

chamber. The gasses were routed via 6mm flexible gas hose tubes from their tanks to the inlet on the plastic mount. The atmosphere is vacated using the pump and is then cross-filled with the pure gas into the chamber.

2.5 Experimental Layout

The overall experimental setup is shown in Figure 2.15, with both the gas and optical components. A photo of the setup is show in Figure 2.16.

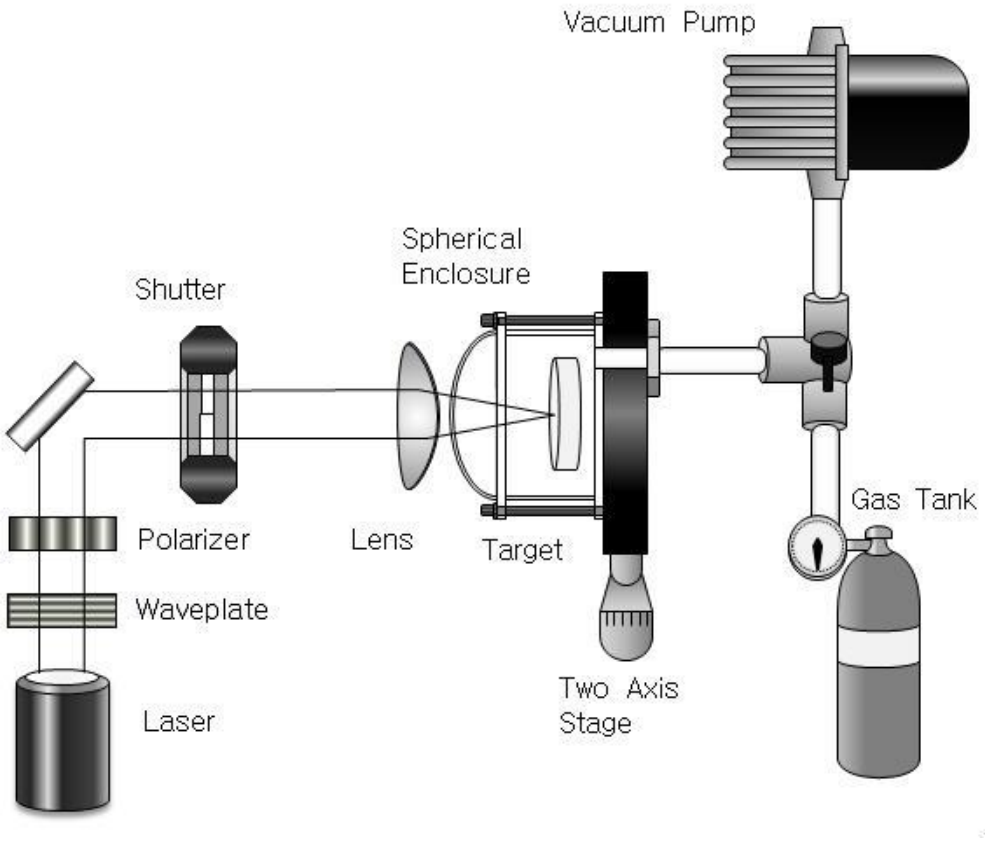

Figure 2. 14: Layout of experimental setup

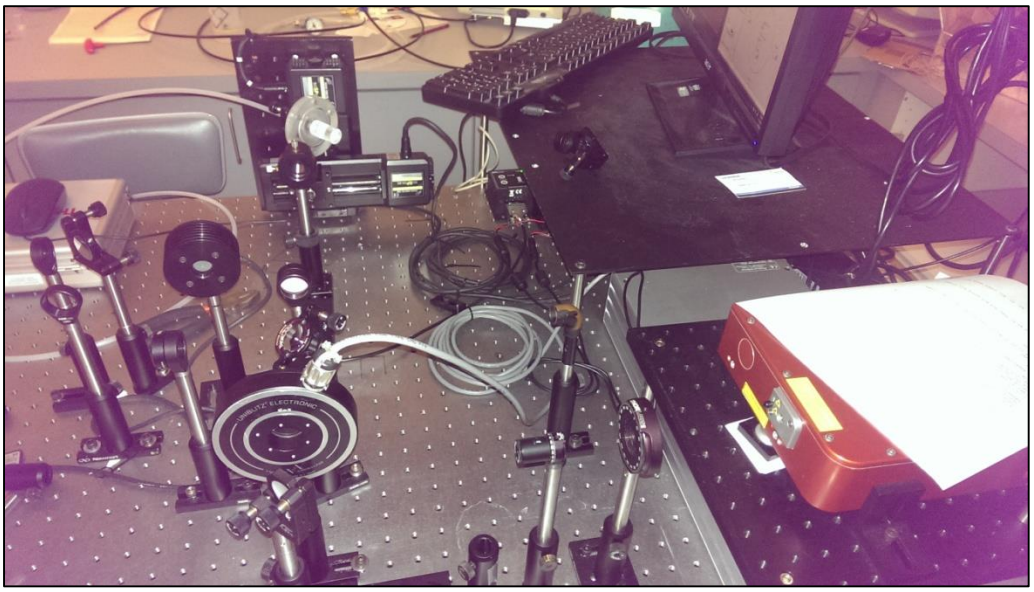

Figure 2. 15: Experimental setup on optics table

2.6 Experimental Procedure

The molybdenum thin films were cut using a glass cutter and reloaded into the ultra-sonicator to be cleaned in an acetone bath. The films were cut into small centimeter-by-centimeter squares to be able to fit onto the target mounts inside the gas chamber. The thin films samples were then attached to the target mounts with double sided tape and pressed flat. Once attached, the samples were cleaned again using acetone and methanol. The mount was then screwed onto the base of the chamber with the all-thread and the hemisphere was then screwed on with the six perimeter bolts. The chamber was then attached to the kinematic mount using a set screw and the mount was placed into the optical base hole mounted onto the two-axis step motors.

The chamber had its atmospheric gas pumped out via the diaphragm vacuum pump. A three-way valve made it possible to close the valve to the pump, and open the valve to the oxygen gas tank. The gas tank valve was then opened and the gas flowed into the chamber at a prescribed and desired pressure. The valve was then closed and the valve to the diaphragm vacuum pump was then opened again and the gas was pumped out. This was repeated ten times to ensure that the air inside the chamber was pumped out and it was replaced with highly concentrated oxygen.

The laser was then turned on and focused onto the sample at a low power in order to not process and oxidize it. It was imperative to check that the laser was focused onto the sample and not the quartz window. Power meter readings taken before the experiments confirmed that the power loss from the laser output to the sample were fairly minimal, accounting for about ~2% losses due to the lens and quartz window.

The goal of the experiment was to determine how changing different variables in pulsed laser processing alter the thin film sample in which ways. This study focuses on how gas pressures as well as exposure times irradiate and oxidize the molybdenum thin films. The variables chosen to study include oxygen pressure, exposure time, and output laser power (fluence). The laser output power was changed in steps of 50 milliwatts between 50 and 600. This accounted for a laser fluence range between 0.25 mJ/cm^2 and 3.53 mJ/cm^2. The exposure timesteps were: 0.05s, 0.5s, 1s, 3s, 5s, 10s, 30s, 60s, and 120s. The exposure times were precisely manipulated via a motorized shutter connected to a lab computer controlled with NI Labview software. The gas pressures were measured

via a compressed gas pressure regulator affixed to the tank. The oxygen gas pressures used were 1 psig, 2psig, 3psig, 4 psig, 8 psig, 12 psig, and 16 psig. It had been shown that different oxygen pressures can alter the different oxides formed in metallic thin films [35]. All experiments were also repeated in ambient air as well for comparison purposes.

Chapter 3: Raman Spectra of Femtosecond Laser Irradiations of Molybdenum Thin Films in Ambient Air

3.1 Introduction

Raman spectroscopy was used to elucidate the resulting oxide rings on the molybdenum thin film after irradiation. The different spectra indicate a trend towards the trioxide being formed in the immediate target area after reaching a specific hypothesized temperature value due to the electron heating from the femtosecond laser. Up until that point, different colorations and phases of the molybdenum dioxide, MoO_2, are seen as exposure time and exposure fluence is increased. Figures 3.1 through Figure 3.6 display both microscopic pictures and the respective Raman spectra of the irradiations for the given fluence and exposure time values depicted.

3.2 Raman Spectroscopy Results

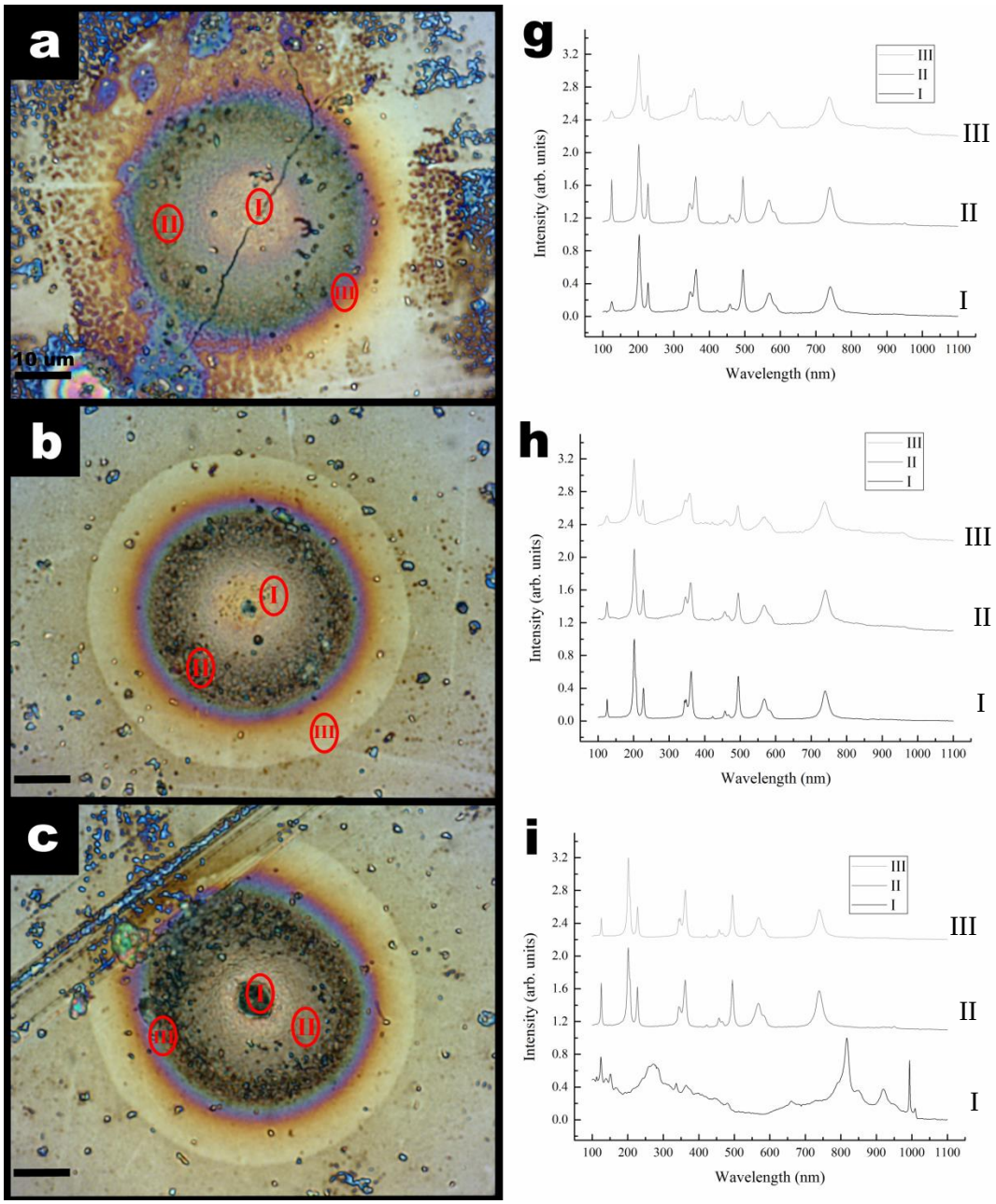

Figure 3. 1: Irradiations of the molybdenum thin film at 100 mW output laser power (fluence: 0.535 mJ/cm2) in air after a) 0.05 seconds b) 0.5 seconds c) 1 seconds and g-i) the respective Raman spectra

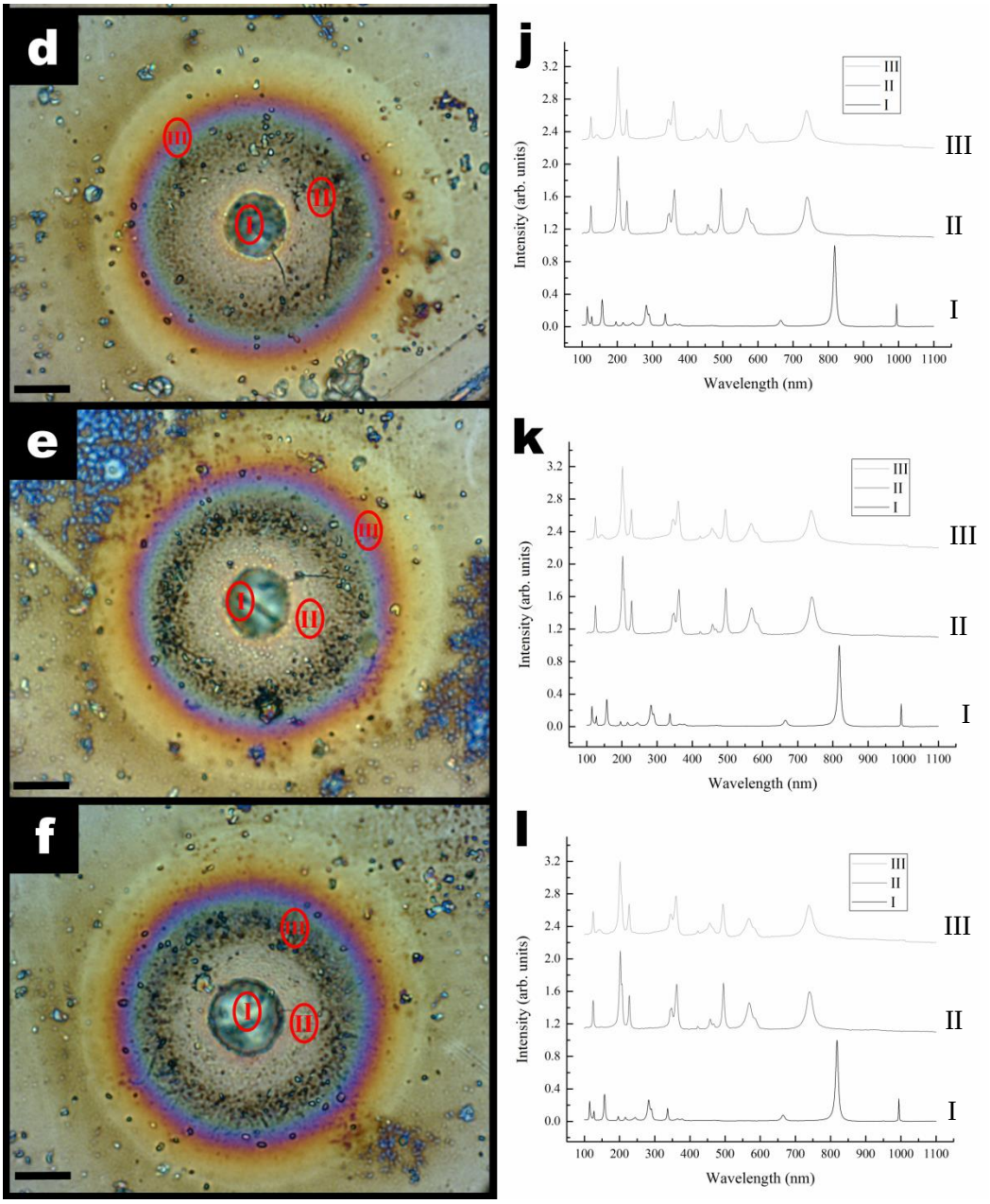

Figure 3. 2: Irradiations of the molybdenum thin film at 100 mW output laser power (fluence: 0.535 mJ/cm2) in air after d) 3 seconds e) 5 seconds f) 10 seconds and j-l) the respective Raman spectra

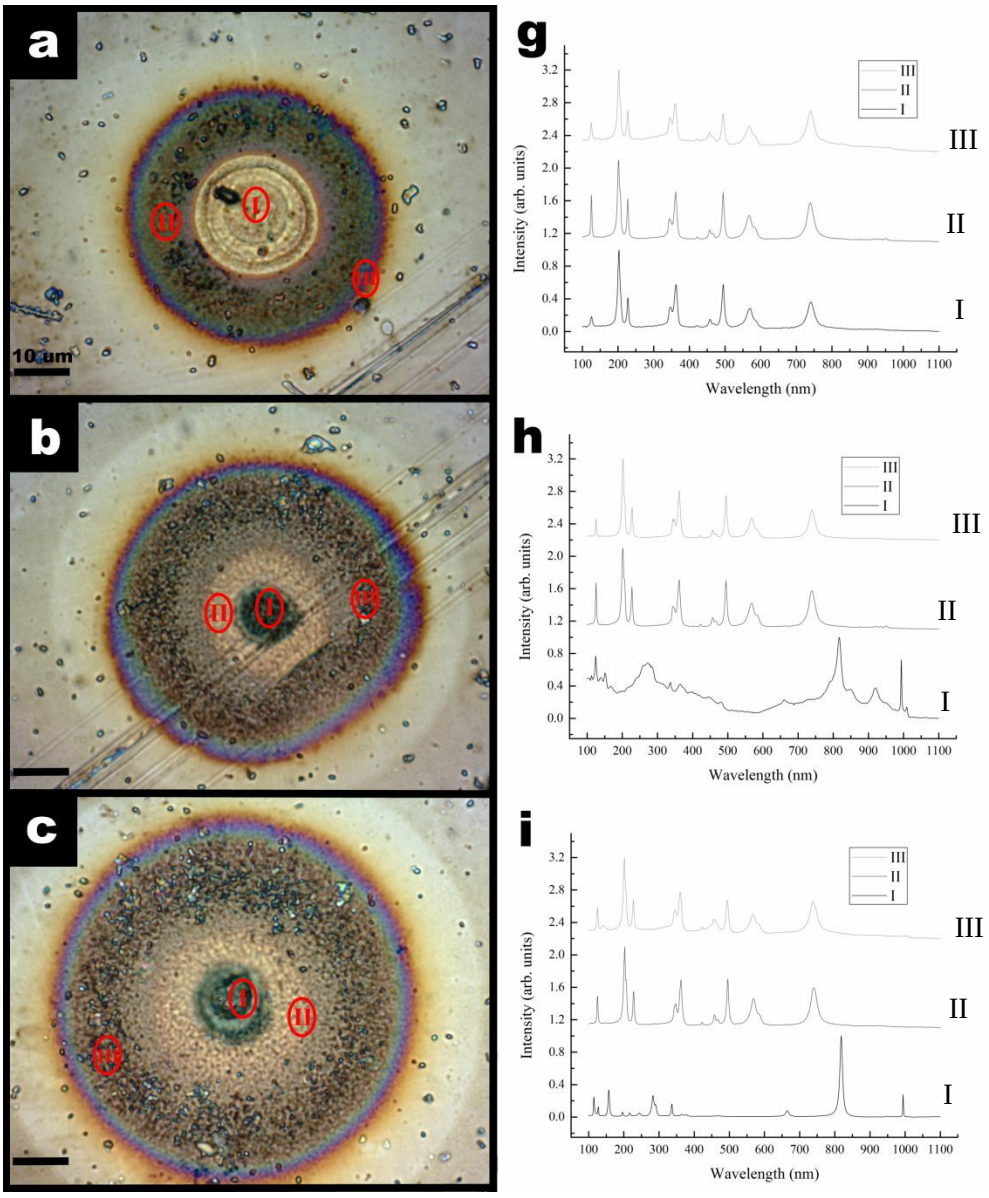

Figure 3. 3: Irradiations of the molybdenum thin film at 200 mW output laser power (fluence: 1.07 mJ/cm2) in air after a) 0.05 seconds b) 0.5 seconds c) 1 seconds and g-i) the respective Raman spectra

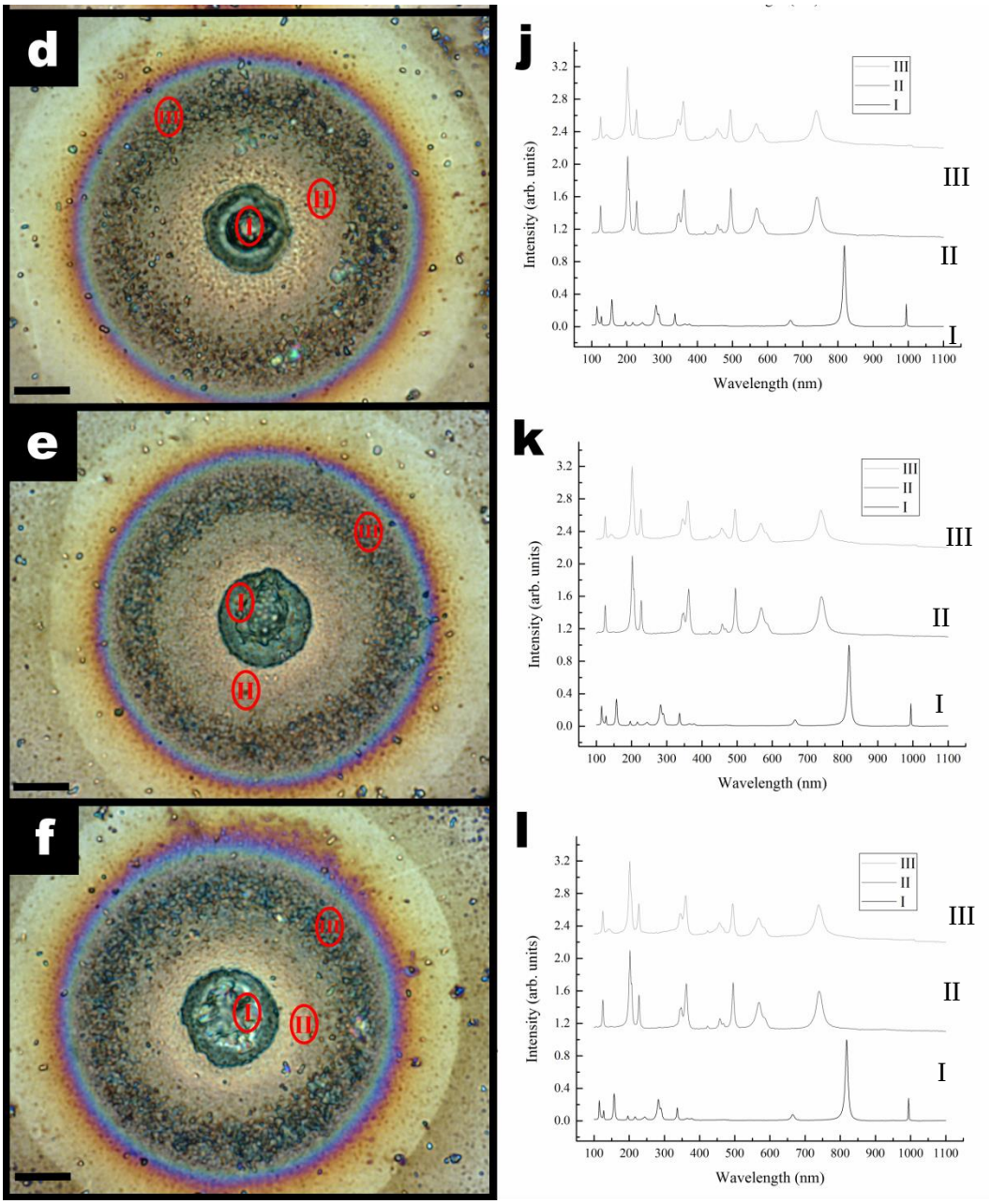

Figure 3. 4: Irradiations of the molybdenum thin film at 200 mW output laser power (fluence: 1.07 mJ/cm2) in air after d) 3 seconds e) 5 seconds f) 10 seconds and j-l) the respective Raman spectra

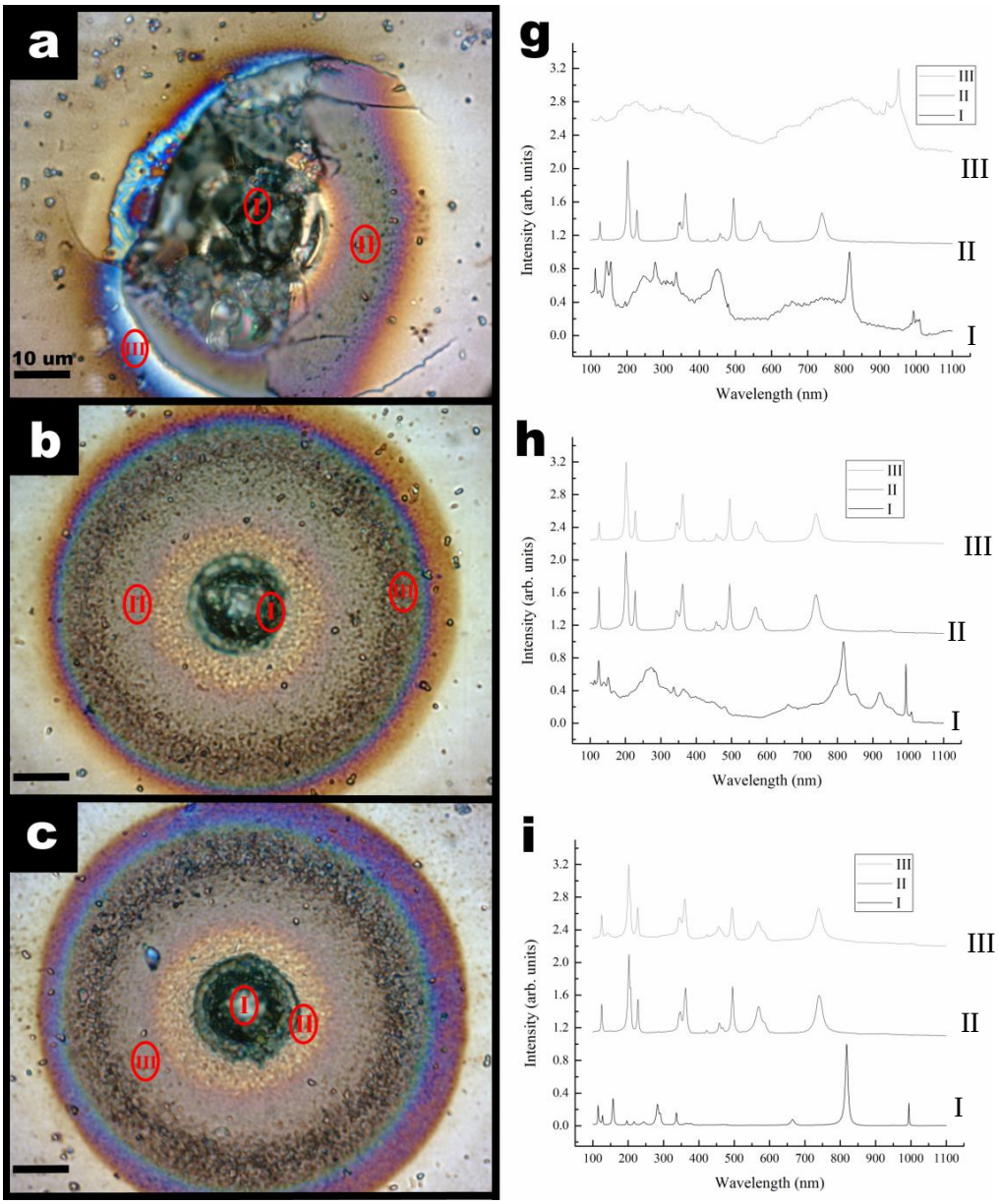

Figure 3. 5: Irradiations of the molybdenum thin film at 400 mW output laser power (fluence: 2.14 mJ/cm2) in air after a) 0.05 seconds b) 0.5 seconds c) 1 seconds and g-i) the respective Raman spectra

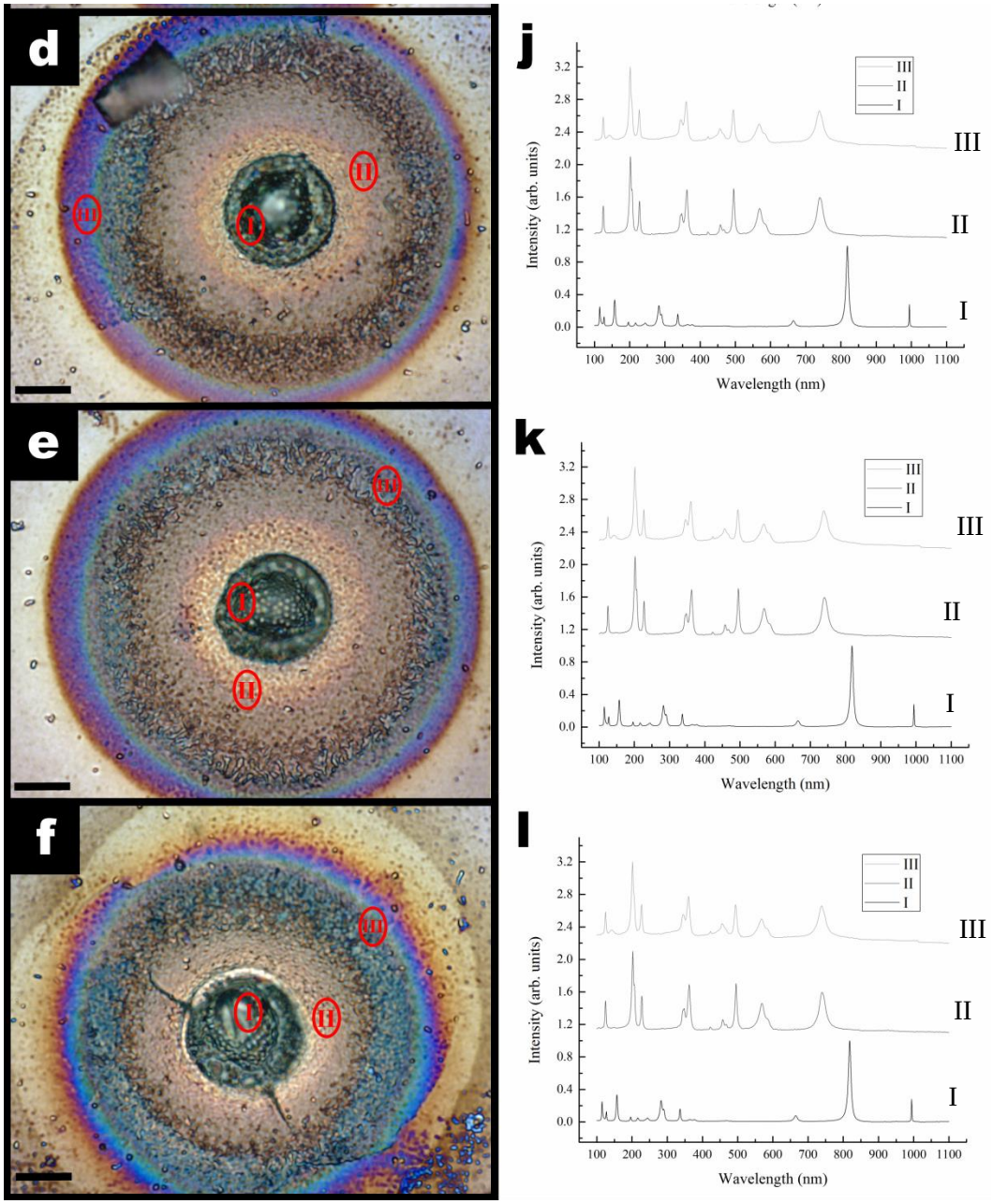

Figure 3. 6: Irradiations of the molybdenum thin film at 400 mW output laser power (fluence: 2.14 mJ/cm2) in air after d) 3 seconds e) 5 seconds f) 10 seconds and j-l) the respective Raman spectra

3.3 Conclusions and Summary

Overall, the trends point to the molybdenum trioxides forming at or around 1 second of irradiation time. Using our only constraint of beam waist, the energy density was calculated for each run based on total output power. As mentioned previously, the output power is very near the sample-irradiated power with very minimal losses going through optical devices. Different colorizations of the dioxides are also shown. This is due to the different temperatures reached via laser heating. Strictly referring to the Raman spectra, it can be seen that zones II and II in most of the images contain the easily distinguishable MoO_2 curves, however, as expected, the intensities of the Stokes lines increase as you get nearer to the irradiated center. This means that the vibrational scattering of the MoO_2 oxide increases as it's subject to higher temperatures.

Specific areas of interest include Figure 3.1c. Here, Raman spectra reveal the beginning and transition of the center irradiated-zone from the molybdenum dioxide into the molybdenum trioxide. This is evidenced by the revealing of the large Stokes lines at around 997 nm, which is a traditional MoO_3 peak. It can be seen that by doubling the fluence, the exposure time needed to obtain this mixed-oxide is effectivity halved, as shown by the spectra in Figure 3.3b. However, doubling the laser fluence from that value doesn't obtain the mixed-oxide quicker, as shown by Figure 3.5b.

Figure 3.4 shows the very minimal spread of the molybdenum trioxide as the exposure time goes from 3 seconds to 5 seconds to 10 seconds. Figure 3.5a is interesting as a whole, as it contains two different identifiable oxide changes. The first one, in zone I,

shows the same transition from MoO_2 to MoO_3 as evidenced by several MoO_3 peaks seen in the spectra, notably around 280 nm, 666 nm, 820 nm, and 997 nm. In the third zone, zone III, the oxidation is caught between the bulk molybdenum spectra showcased initially in Figure 2.2 and the initial stages of dioxide formation, as evident by the MoO_2 peak beginning to show at around 950 nm.

Chapter 4: Raman Study of Femtosecond Laser Irradiations of Molybdenum Thin Films in Oxygen Gas

4.1 Introduction

From Raman spectroscopy, it can be seen that the peaks from the spectra taken in the outer rings highly correlate with traditionally reported monoclinic dioxide m-MoO_2 Raman peaks. Peaks at 203, 228, 345, 363, 461, 495, 571, 589, 744 cm^{-1} agree with Raman spectra of m-MoO_2; similarly, peaks at 245, 284, 338, 365, 472, 666, 820, 996 cm^{-1}, taken in the middle target zone of the irradiations, match up with known spectra of the α-MoO_3 trioxide [36–39]. These trioxide results are tabulated in Table 4.1 for the varying pressure differences as well as against external sources. From Table 4.1, it can be seen that the trioxide peaks still form in line with previously reported results for the given vibrational modes.

Table 4. 1: Molybdenum trioxide Raman frequencies (cm^{-1})

MoO_3 This work air	MoO_3 This work 1 psi	MoO_3 This work 2 psi	MoO_3 This work 3 psi	MoO_3 This work 4 psi	MoO_3 This work 8 psi	MoO_3 This work 12 psi	MoO_3 This work 16 psi	MoO_3 M. Camacho-Lopez [37]	MoO_3 Blume [36]	MoO_3 Commercial [37]
	216		216		216	218	215	211	218	217
284	286	288	286	281	281	280	282	283	284	284
	291	290					290		292	291
337	337	337	338	336	336	336	336	336	338	338
	366		365	372	369	370	378	364	366	365
	483	483	483					468	472	472
664	671		672	665	665	663	665	662	665	666
819	818	821	822	817	818	812	818	819	820	820
995	997	997	997	994	995	995	995	992	996	996

4.2 Raman Spectroscopy Results

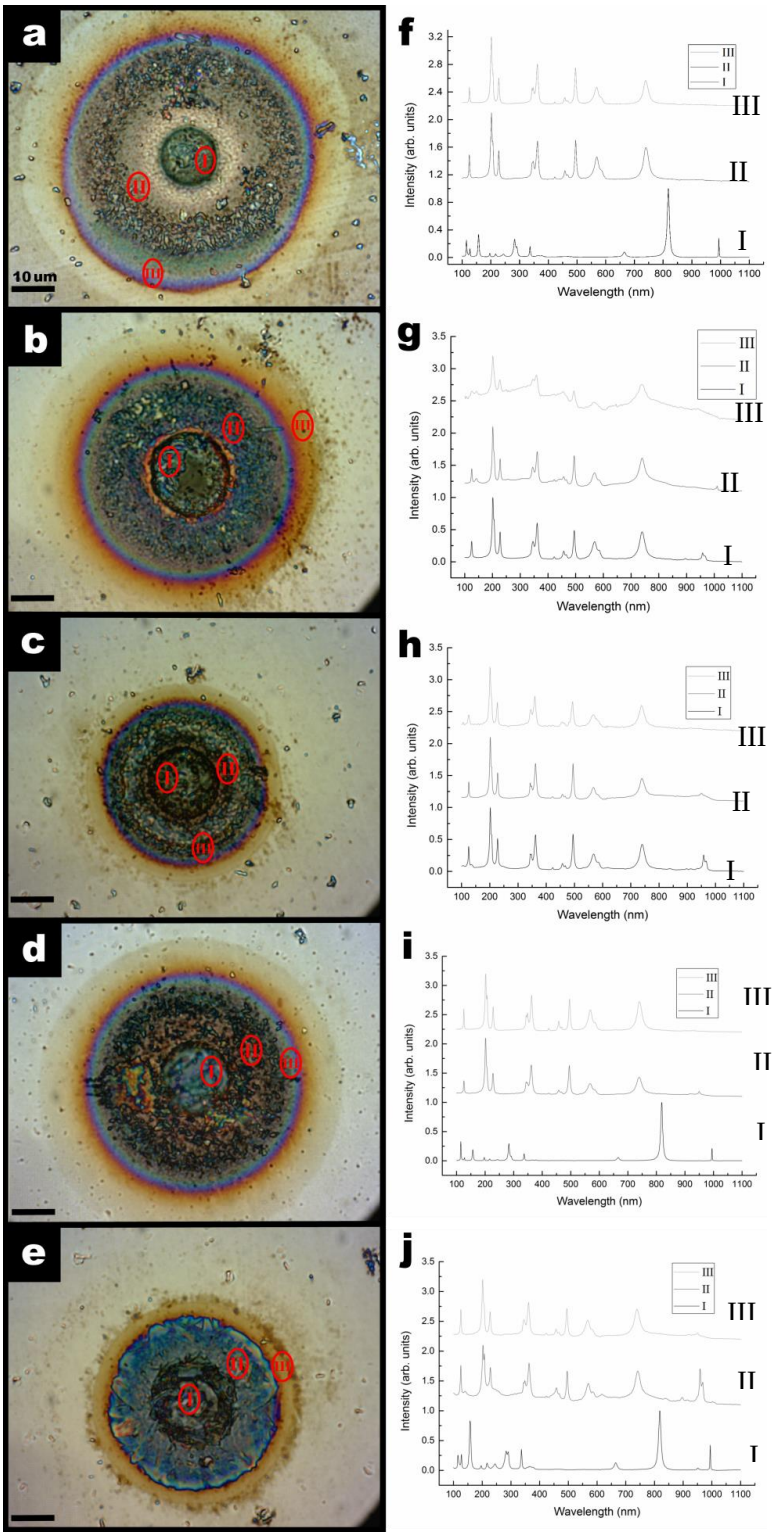

Figure 4. 1: Irradiations of the molybdenum thin film at 150 mW output laser power (fluence: 0.802 mJ/cm2) for 10 seconds a) in air b) in 4 psi of oxygen c) in 8 psi of oxygen d) in 12 psi of oxygen e) in 16 psi of oxygen and f-j) the respective Raman spectra

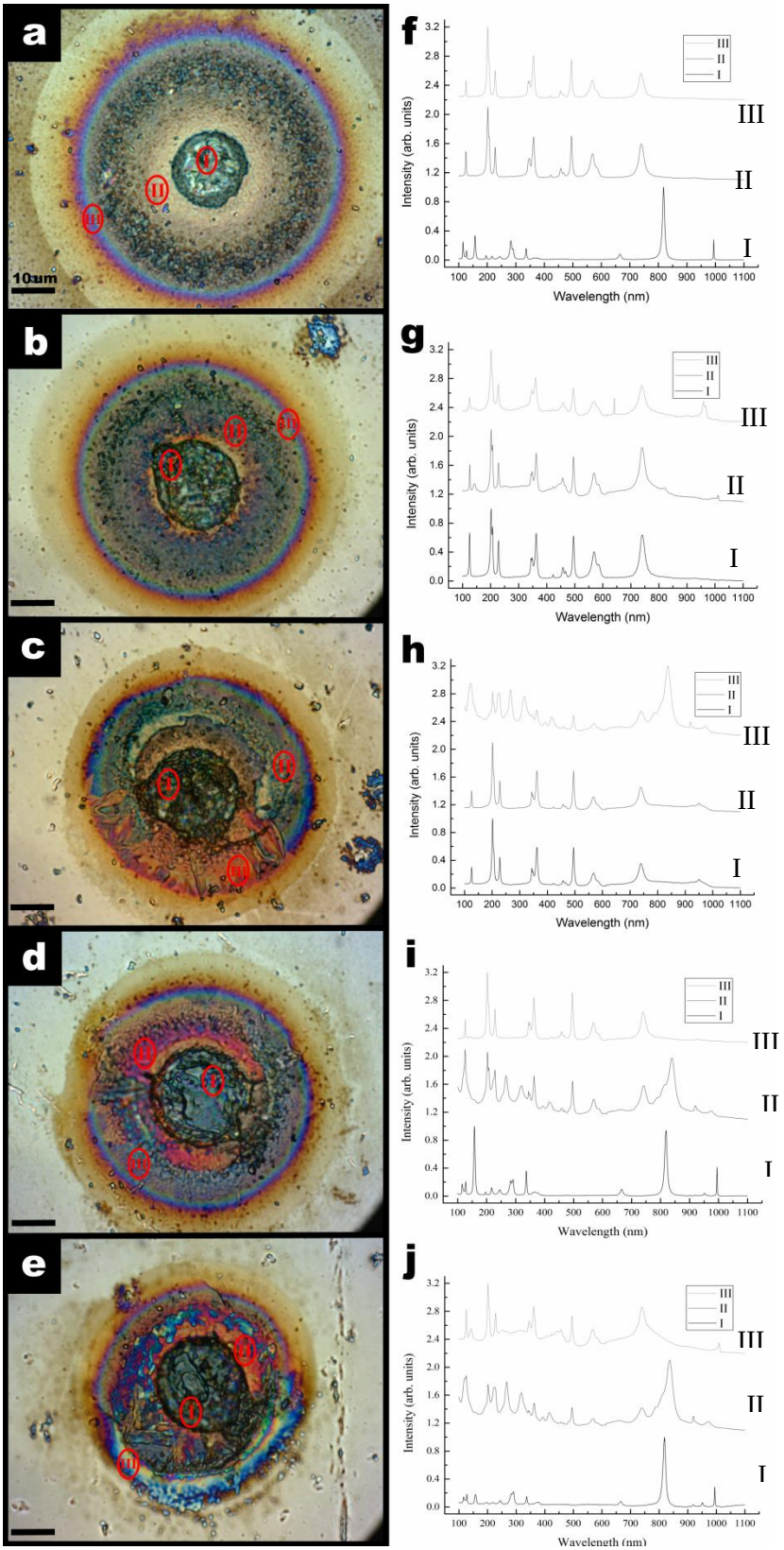

Figure 4. 2: Irradiations of the molybdenum thin film at 200 mW output laser power (fluence: 1.07 mJ/cm2) for 10 seconds a) in air b) in 4 psi of oxygen c) in 8 psi of oxygen d) in 12 psi of oxygen e) in 16 psi of oxygen and f-j) the respective Raman spectra

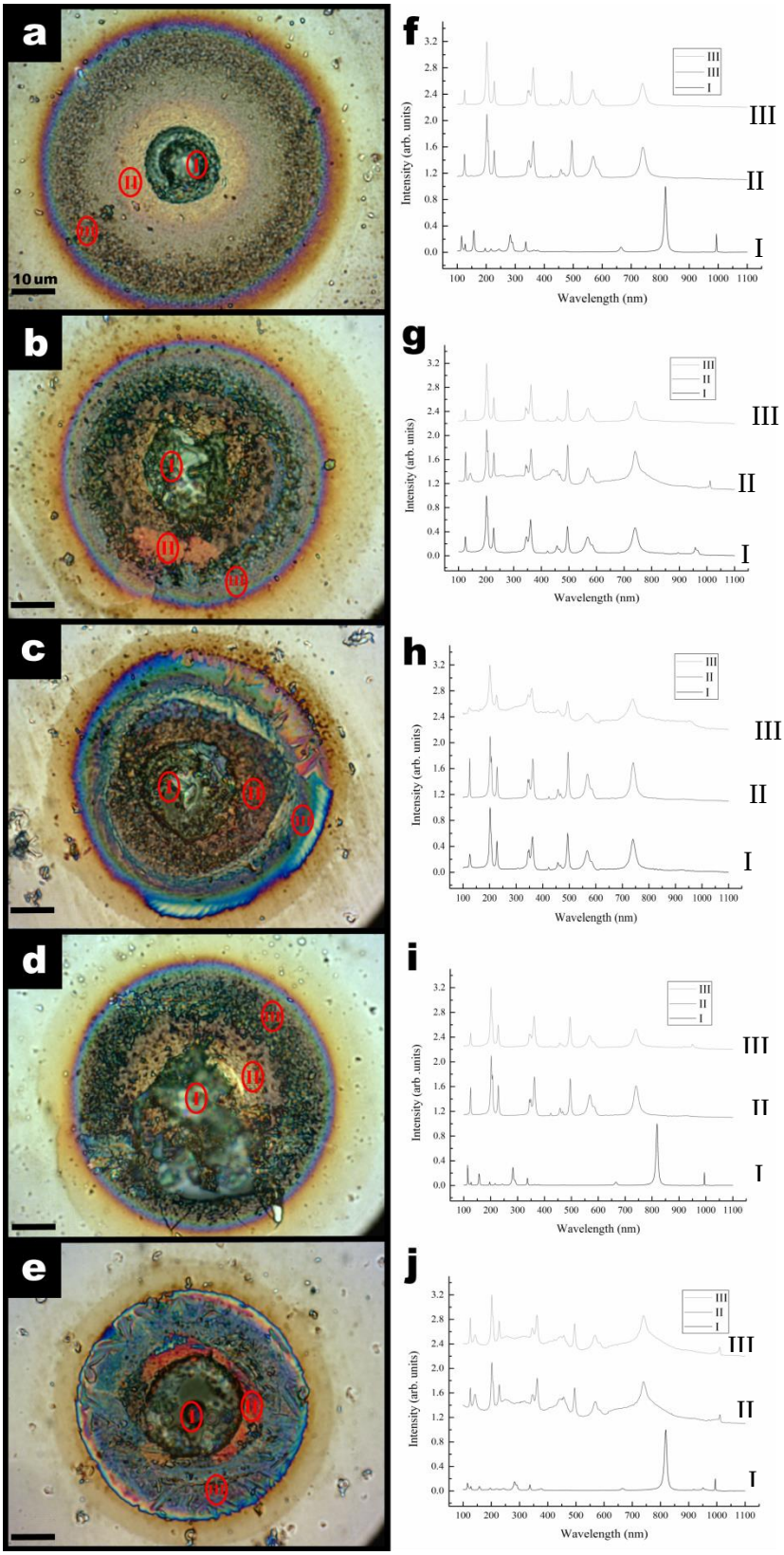

Figure 4. 3: Irradiations of the molybdenum thin film at 300 mW output laser power (fluence: 1.6 mJ/cm2) for 1 second a) in air b) in 4 psi of oxygen c) in 8 psi of oxygen d) in 12 psi of oxygen e) in 16 psi of oxygen and f-j) the respective Raman spectra

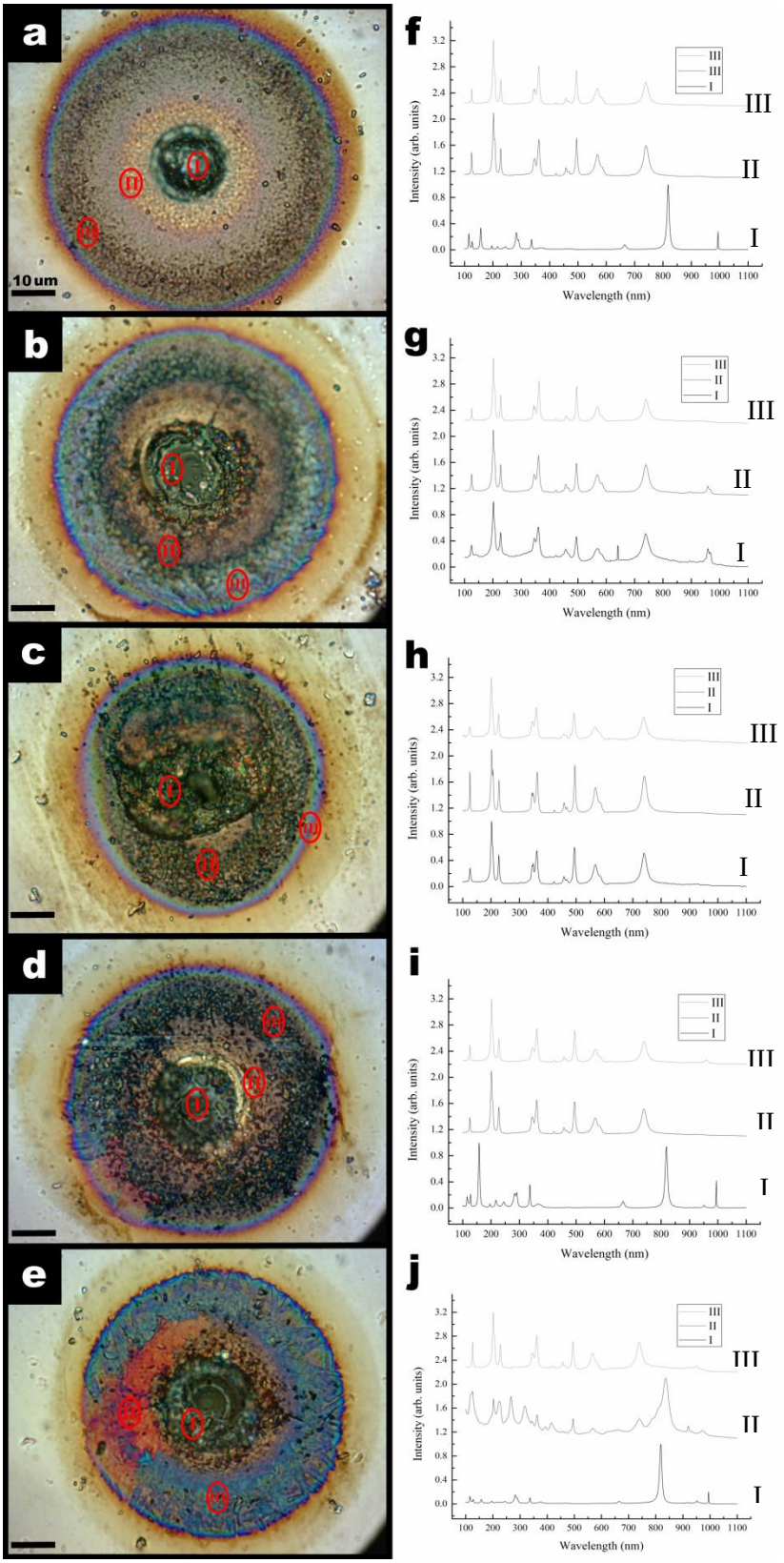

Figure 4. 4: Irradiations of the molybdenum thin film at 400 mW output laser power (fluence: 2.14 mJ/cm2) for 0.5 seconds a) in air b) in 4 psi of oxygen c) in 8 psi of oxygen d) in 12 psi of oxygen e) in 16 psi of oxygen and f-j) the respective Raman spectra

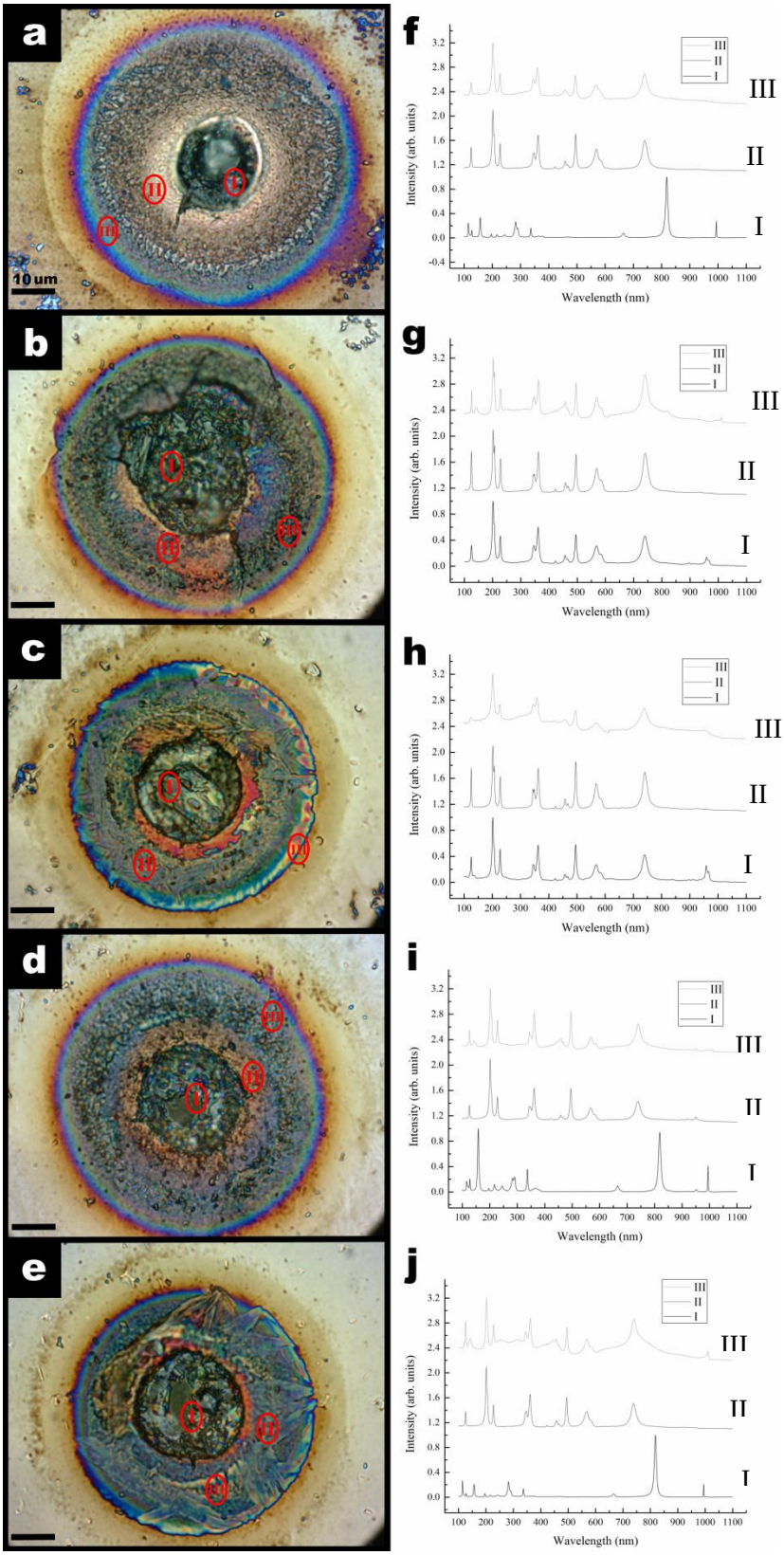

Figure 4. 5: Irradiations of the molybdenum thin film at 400 mW output laser power (fluence: 2.14 mJ/cm2) for 10 seconds a) in air b) in 4 psi of oxygen c) in 8 psi of oxygen d) in 12 psi of oxygen e) in 16 psi of oxygen and f-j) the respective Raman spectra

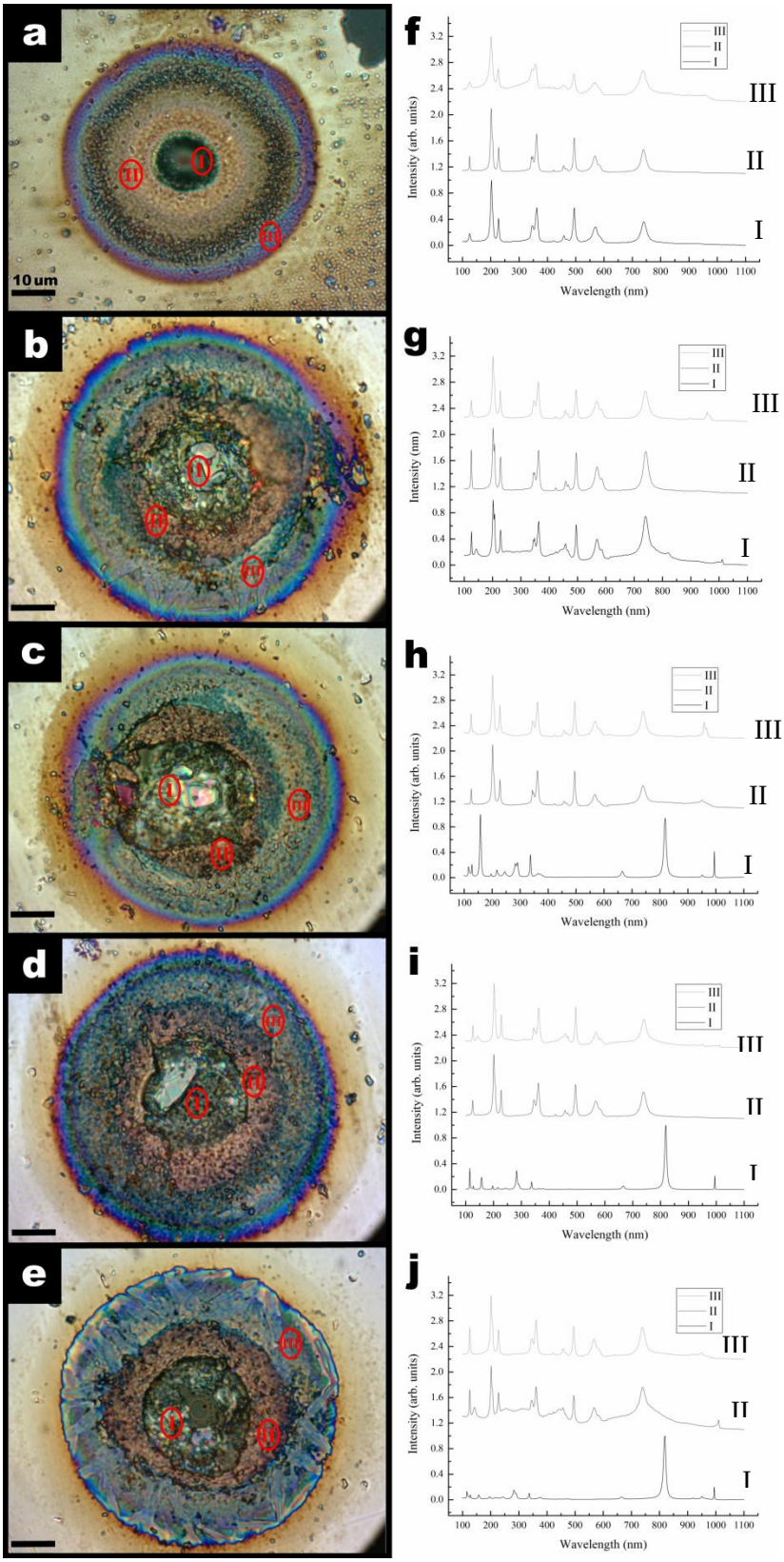

Figure 4. 6: Irradiations of the molybdenum thin film at 600 mW output laser power (fluence: 3.21 mJ/cm2) for 0.5 seconds a) in air b) in 4 psi of oxygen c) in 8 psi of oxygen d) in 12 psi of oxygen e) in 16 psi of oxygen and f-j) the respective Raman spectra

4.3 Trioxide Formation Extent and Size

A comprehensive review of every irradiation site was done in order to determine the extent of trioxide formation when exposed to oxygen at the given parameters. The goal was to see how changing the gas and pressure conditions altered the area and diameter of the α-MoO_3 oxide at the immediate irradiation zone. Extensive measurements done with Optical Microscopy were processed. This data, for the representative fluences of 1.17 mJ/cm^2 and 3.23 mJ/cm^2, are shown in Fig. 4.8. It can be seen that with the introduction of a pressurized oxygen gas, the overall area of the α-MoO_3 formation is greatly increased with minimal increases in pressure. This tells us that by increasing the oxygen concentration, with additional increases in oxygen pressure, the molybdenum thin film oxidizes more for the given exposure times and fluences. This can be attributed to two things, the increase in pressure is directly proportional to the diffusion rate, thereby having an increased diffusion rate, and faster oxygen atoms are therefore diffused into the thin film when heated with the laser. The second explanation is related to the atmospheric composition of the local gas; ambient air is approximately 20% oxygen by volume. The more oxygen atoms present, the more oxygen particles are transferred through the passive oxide layer and the more metal-oxygen particle interactions there are, resulting in the growth of the oxide.

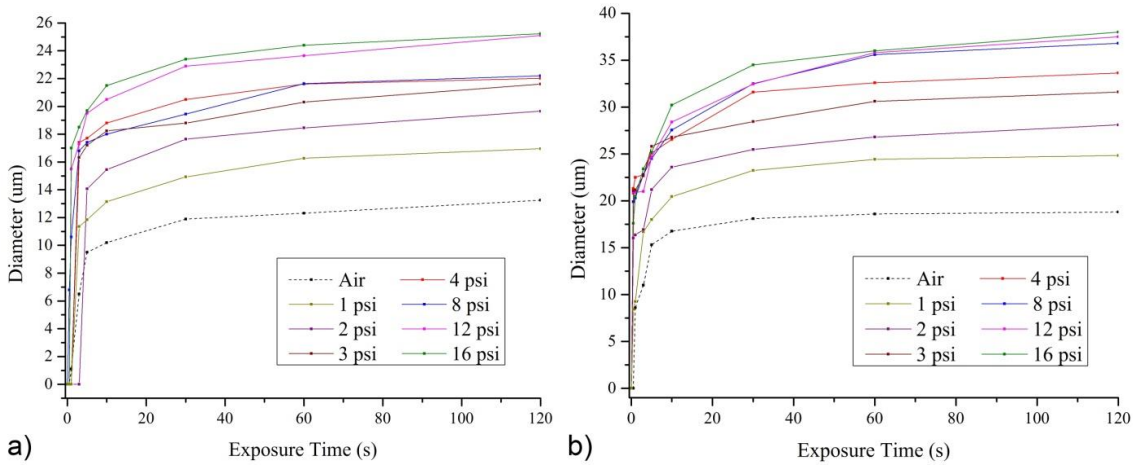

Figure 4. 7: Molybdenum trioxide formation diameter for 10s exposure at a) 1.17 mJ/cm2 and b) 3.23 mJ/cm2 fluence for each atmospheric condition

4.4 Dioxide Topographical Structure Characterization

When testing for phase and composition under Raman microscopy, it was seen that the Raman laser was going in and out of focus in different oxidation zones. This could be due to several things. One, it could imply that the different resulting oxidation rings can be higher and lower physically than each other and opened the door for exploration and explanation. It could also mean the trioxide formations were creeping under the dioxide. Different methodology was applied to be able to decipher these topographically diverse formations. First, SEM images were taken of the irradiation sites to confirm the differing bumps and regions. The samples were then taken to a Focused Ion Beam (FIB) machine to be able to carefully scratch away some of the metal. The goal of this was to be able to see what happens under the surface of the oxide zones. The samples were then placed, at an angle, back into a SEM and images were taken. Fig. 4.9 shows FIB-cut irradiation zones.

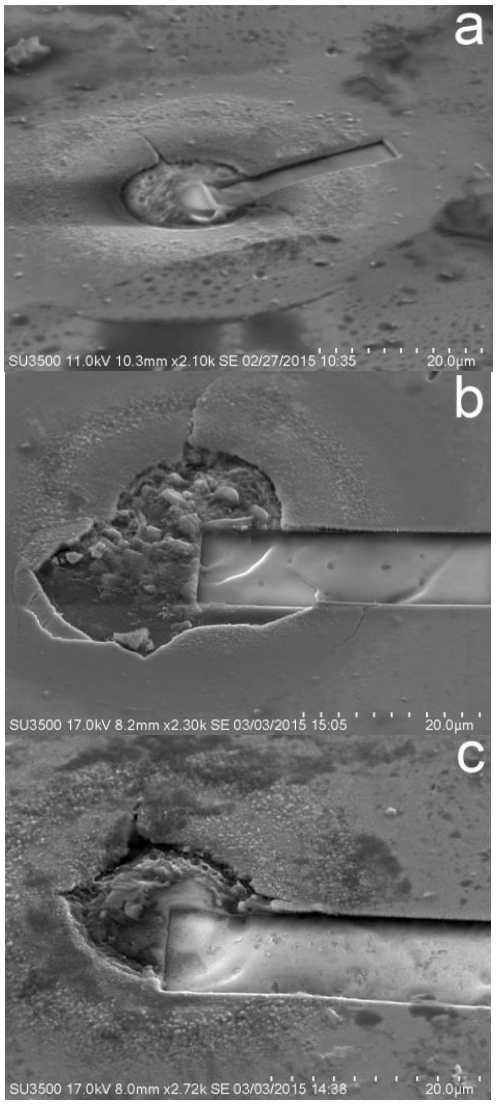

Figure 4. 8: Scanning electron microscope images for 10s irradiations at 2.35 mJ/cm^2 in a) ambient air b) 4psi oxygen and c) 12 psi oxygen

It is seen from the resulting SEM and FIB-ran SEM images that the dioxide zone and rings rise above the thin film as it's oxidized. The zone in the middle, the α-MoO_3, also depresses well below the neighboring m-MoO_2 and creates an identifiable crater area. From these images, it was decided to do an atomic force microscopy study to

identify how high the m-MoO_2 formations areas rise and how changing the fluence, exposure time, and gas atmospheres alter these surface features.

4.5 Thermal Treatment Comparison

An important facet when discussing the formation of these oxides is how pulsed laser processing compares against traditional thermal treatments of metallic thin films. The oxides seen in this study have been replicated in thermal heating experiments, both in preliminary studies by our group and others [40]. The specific temperatures needed to reach desired oxides fall into known, reported ranges [41,42]. Initial measurements taken by infrared detecting devices by our group show that the laser heating process falls into the stated temperature ranges; detailed insights are still underway. However, several conclusions can still be made when relating these two thin film oxidation methods. Firstly, the timescales involved make pulsed laser processing very desirable. The time it takes some of these oxidations occur can be up to several hours – not to mention the time it takes for ovens to ramp up and cool down. Secondly, the thermal oxidation in an oven would occur as a homogenous sheet. Since the whole sample is being heated, the whole sample is oxidizing. Because of this, the morphology and structure of the resulting oxides should also be mostly consistent. In pulsed laser processing, the laser can focus down to very small and focused areas, leaving the non-effected area of the thin films largely unaffected. The tunability of pulsed laser processing is another benefit that can extend to a laser's use in oxidizing metallic thin films, not requiring the oxidation of the whole sample with traditional thermal treatments.

With the correct fluences, exposure time, and now gas concentration, pulsed laser oxidation of transition metal thin films can be a very viable method of obtaining desired oxides. Using stages and controllers, precise fabricating and patterning is also very attainable and can open up very interesting options in the micro- and nanoscale. While we have shown the oxides attained with pulsed laser processing are comparable to thin film oxides formed with other methods, the exact optical and electrical properties of the oxides formed in the pressurized oxygen gas environments are still being measured.

4.6 Conclusions and Summary

The introduction of oxygen gas into the immediate atmosphere near the target zone shows several clear trends. For one, the trioxide formation is able to expand more in higher pressures with the same fluence. Comparing "a" and "d/e" in each of the figures demonstrate this. Another identifiable trend is the overall homogeneity of the dioxides, focusing on the outlying zones II and III of the figures in this chapter. In the air trials, very strong MoO_2 Stokes lines are present. As oxygen gas is introduced, these lines get less and less pronounced, and faint MoO_3 Stokes lines begin to appear. Comparing the images and spectra of Figure 4.1deij, Figure 4.2deij, and Figure 4.3deij, it can be concluded that as oxygen concentration increases and more oxygen ions are present in the thin film-gas boundary, more oxygen ions are able to diffuse into the vacancy sites as the

metal is heated with the laser, resulting in more widespread trioxide formation and more mixed-oxide zones when compared against irradiating the samples in air.

Somewhere between the output fluences of 2.14 mJ/cm^2 and 3.21 mJ/cm^2 does the laser heat the molybdenum thin film sample enough as to where the central, irradiated zone goes from a mixed-oxide phase to the trioxide in 8psi oxygen gas. This is shown by comparing Figure 4.5ch with Figure 4.6ch.

Chapter 5: Conclusions and Future Work

5.1 Conclusions

This work demonstrates the phase and formation changes of femtosecond laser irradiations on molybdenum thin films and the comparison between doing the irradiations in ambient air versus different oxygen pressure conditions. High speed (54 MHz), low energy (20nJ), femtosecond pulse-width (230 fs) lasers were shown to oxidize molybdenum thin films and form monoclinic MoO_2 and orthorhombic MoO_3 in different areas of the irradiated region and its surroundings. Furthermore, the introduction of a gaseous oxygen environment of varying pressures drastically altered the necessary power and exposure times required to form the specific oxides in comparison to the oxides in ambient air. Even in the low chamber pressure conditions studied, the α-MoO_3 formed to a greater extent and with lower exposure parameters than the irradiations done in the ambient air atmosphere with the exact same irradiation specifics.

5.2 Future Work

As has been discussed, there is much room to expand the investigation of transition metal oxide formations due to laser-irradiations. First and foremost, it would be trivial to expand these studies to other gases and other transition metals. Preliminary studies have shown similar laser-induced oxidations in titanium, zinc, bismuth, and chromium. To the author's knowledge, the varying of gaseous environments have yet to be published for any of these transition metal thin films due to laser irradiations. Argon

and nitrogen gases are of interest due to the different applications each can include. Similarly, higher pressures in the chambers can afford some interesting experimentation. Due to the design limitation of the chamber used in this research study, higher pressures weren't able to be reached without compromising the integrity and safety of the chamber, sample, and optics equipment.

With regards to the physics at play, it would be very interesting to design an experiment to be able to decipher how the laser-material interactions and oxidation occur. Due to the short thermal diffusion time but even shorter electron-interaction time, it is still unknown what realm of physics dominate the oxidation of these metallic thin films. By irradiating the thin film with as many low-energy pulses as possible before the thermal diffusion time, one can see what physical phenomenon dominate the oxidation kinematics of this intriguing material processing.

Raman analysis can be furthered with the current results to be able to determine if there is a distinguishable Raman shift with the changing parameters. One would need to make sure to use the exact same Raman spectra parameters when comparing the resulting spectra to be able to determine the exact phases and vibrational modes for each test site.

Other expansions of this project, once the physics is determined, can be to be able to model the laser-heating effects. This is non-trivial due to the material changing and altering from the laser pulses. This can be started once it is determined whether the heating from the laser pulses are thermal, non-thermal, or the currently accepted ration that it is due to some degree of both.

Further work can amount to the refined processing and implementation of the oxidation of molybdenum thin films. The trioxide has some interesting optical and electrical properties which have already showed promise in gas sensors and solar cells, to name a few. Once we are able to dominate the formation of these oxides and characterize their optical, electrical, and thermal properties, real-world applications begin to become a possibility.

References

[1] C. V. Ramana and C. M. Julien, “Chemical and electrochemical properties of molybdenum oxide thin films prepared by reactive pulsed-laser assisted deposition,” *Chem. Phys. Lett.*, vol. 428, no. 1–3, pp. 114–118, 2006.

[2] J. Scarminio, a. Lourenço, and a. Gorenstein, “Electrochromism and photochromism in amorphous molybdenum oxide films,” *Thin Solid Films*, vol. 302, no. 1–2, pp. 66–70, 1997.

[3] O. Zelaya-Angel, C. Menezes, F. Sanchez-Sinencio, and G. F. L. Ferreira, “ELECTRON DIFFUSION AND ELECTROCHROMISM IN MoO//3 AMORPHOUS FILMS.,” *J. Appl. Phys.*, vol. 51, no. 11, pp. 6022–6026, 1980.

[4] S. H. Lee, Y. H. Kim, R. Deshpande, P. a. Parilla, E. Whitney, D. T. Gillaspie, K. M. Jones, a. H. Mahan, S. Zhang, and A. C. Dillon, “Reversible lithium-ion insertion in molybdenum oxide nanoparticles,” *Adv. Mater.*, vol. 20, no. 19, pp. 3627–3632, 2008.

[5] K. Gesheva, a. Szekeres, and T. Ivanova, “Optical properties of chemical vapor deposited thin films of molybdenum and tungsten based metal oxides,” *Sol. Energy Mater. Sol. Cells*, vol. 76, no. 4, pp. 563–576, 2003.

[6] Y. Zhang, S. Kuai, Z. Wang, and X. Hu, “Preparation and electrochromic properties of Li-doped MoO 3 films fabricated by the peroxo sol – gel process,” *Appl. Surf. Sci.*, vol. 165, pp. 56–59, 2000.

[7] M. Cano-Lara, S. Camacho-López, a. Esparza-García, and M. a. Camacho-López, “Laser-induced molybdenum oxide formation by low energy (nJ)–high repetition rate (MHz) femtosecond pulses,” *Opt. Mater. (Amst).*, vol. 33, no. 11, pp. 1648–1653, Sep. 2011.

[8] V. P. Veiko, M. V. Yarchuk, and a. I. Ivanov, “Mechanisms of thin Cr fimls modification under multipilse femtosecond laser action,” in *SPIE*, 2010, vol. 7996, pp. 799607–799607–6.

[9] V. P. Veiko, M. V. Yarchuk, and a. I. Ivanov, “Study of low-threshold mechanisms for modifying the structure of thin chromium films under the action of supershort laser pulses,” pp. 512–518, 2011.

[10] G. R. Castillo-vega, E. H. Penilla, S. Camacho-lópez, G. Aguilar, and J. E. Garay, “Waveguide-like structures written in transparent polycrystalline ceramics with an ultra-low fluence femtosecond laser,” vol. 2, no. 10, pp. 1416–1424, 2012.

[11] K. Sugioka and Y. Cheng, *Femtosecond Laser 3D Micromachining for Microfluidic and Optofluidic Applications*. Springer Briefs in Applied Sciences and Technology, 2014.

[12] M. Rouhani, Y. L. Foo, J. Hobley, J. Pan, G. S. Subramanian, X. Yu, A. Rusydi, and S. Gorelik, "Photochromism of amorphous molybdenum oxide films with different initial Mo5+ relative concentrations," *Appl. Surf. Sci.*, vol. 273, pp. 150–158, 2013.

[13] M. Rouhani, J. Hobley, G. S. Subramanian, I. Y. Phang, Y. L. Foo, and S. Gorelik, "The influence of initial stoichiometry on the mechanism of photochromism of molybdenum oxide amorphous films," *Sol. Energy Mater. Sol. Cells*, vol. 126, pp. 26–35, Jul. 2014.

[14] G. Heise, M. Englmaier, C. Hellwig, T. Kuznicki, S. Sarrach, and H. P. Huber, "Laser ablation of thin molybdenum films on transparent substrates at low fluences," *Appl. Phys. A Mater. Sci. Process.*, vol. 102, no. 1, pp. 173–178, 2011.

[15] D. Di Yao, J. Z. Ou, K. Latham, S. Zhuiykov, A. P. O. Mullane, and K. Kalantar-zadeh, "Electrodeposited α - and β -Phase MoO 3 Films and Investigation of Their Gasochromic Properties," 2012.

[16] S. . Sunu, E. Prabhu, V. Jayaraman, K. . Gnanasekar, T. . Seshagiri, and T. Gnanasekaran, "Electrical conductivity and gas sensing properties of MoO31," *Sensors Actuators B Chem.*, vol. 101, no. 1–2, pp. 161–174, Jun. 2004.

[17] D. V Ahire, S. D. Shinde, G. E. Patil, K. K. Thakur, V. B. Gaikwad, V. G. Wagh, G. H. Jain, and V. N. N. Arts, "PREPARATION OF MoO 3 THIN FILMS BY SPRAY PYROLYSIS AND ITS GAS SENSING PERFORMANCE," *Int. J. Smart Sens. Intell. Syst.*, vol. 5, no. 3, pp. 592–605, 2012.

[18] W. Xue, C. Wang, H. Tian, and Y. Lai, "Corrosion behaviors and galvanic studies of microarc oxidation films on Al–Zn–Mg–Cu alloy," *Surf. Coatings Technol.*, vol. 201, no. 21, pp. 8695–8701, Aug. 2007.

[19] J. S. Fang and Y. T. Chen, "Passivation of copper–hafnium thin films using self-forming hafnium oxide," *Surf. Coatings Technol.*, vol. 231, pp. 166–170, Sep. 2013.

[20] "Oxidation Factsheet." [Online]. Available: http://www.rolledalloys.com/dotAsset/e702f59e-7e60-4331-ac0e-fac8c29fba91.pdf. [Accessed: 23-Mar-2015].

[21] M. S. Aida, E. Tomasella, J. Cellier, M. Jacquet, N. Bouhssira, S. Abed, and a. Mosbah, "Annealing and oxidation mechanism of evaporated zinc thin films from zinc oxide powder," *Thin Solid Films*, vol. 515, no. 4, pp. 1494–1499, Dec. 2006.

[22] "USGS Fact Sheet 2009-3106: Molybdenum—A Key Component of Metal Alloys." [Online]. Available: http://pubs.usgs.gov/fs/2009/3106/. [Accessed: 23-Mar-2015].

[23] S. Lee, H. M. Cheong, P. Liu, D. Smith, C. E. Tracy, A. Mascanrenhas, J. R. Pitts, and S. K. Deb, "Gasochromic mechanism in a -WO 3 thin films based on Raman spectroscopic studies," *J. Appl. Phys.*, vol. 88, no. September, pp. 3076–3078, 2000.

[24] M. a. Camacho-López, E. Haro-Poniatowski, L. Lartundo-Rojas, J. Livage, and C. M. Julien, "Amorphous-crystalline transition studied in hydrated MoO3," *Mater. Sci. Eng. B Solid-State Mater. Adv. Technol.*, vol. 135, no. 2, pp. 88–94, 2006.

[25] S. H. Lee, M. J. Seong, C. E. Tracy, A. Mascarenhas, J. R. Pitts, and S. K. Deb, "Raman spectroscopic studies of electrochromic a-MoO3 thin films," *Solid State Ionics*, vol. 147, no. 1–2, pp. 129–133, 2002.

[26] K. Galatsis, Y. X. Li, W. Wlodarski, and E. Comini, "Semiconductor MoO 3 ± TiO 2 thin ® lm gas sensors," *Sensors Actuators B*, vol. 77, no. 2, pp. 472–477, 2001.

[27] H. M. Martínez, J. Torres, M. E. Rodríguez-García, and L. D. López Carreño, "Gas sensing properties of nanostructured MoO3 thin films prepared by spray pyrolysis," *Phys. B Condens. Matter*, vol. 407, no. 16, pp. 3199–3202, Aug. 2012.

[28] J. Hermann, M. Benfarah, G. Coustillier, S. Bruneau, E. Axente, J.-F. Guillemoles, M. Sentis, P. Alloncle, and T. Itina, "Selective ablation of thin films with short and ultrashort laser pulses," *Appl. Surf. Sci.*, vol. 252, no. 13, pp. 4814–4818, Apr. 2006.

[29] A. S. Khanna, *Introduction to High Temperature Oxidation and Corrosion*. ASM International, 2002.

[30] A. F. Christiansen, H. Fjellvåg, A. Kjekshus, and B. Klewe, "Synthesis and characterization of molybdenum(VI) oxide sulfates and crystal structures of two polymorphs of MoO2(SO4)," *J. Chem. Soc. Dalt. Trans.*, no. 6, pp. 806–815, Jan. 2001.

[31] "BALSAC Chemical picture gallery." [Online]. Available: http://www.fhi-berlin.mpg.de/KHsoftware/Balsac/pictures.html. [Accessed: 23-Mar-2015].

[32] S. Bialkowski, *Photothermal Spectroscopy Methods for Chemical Analysis*. John Wiley & Sons, 1996.

[33] "DirectVacuum.com - Magnetron Sputtering Technology." [Online]. Available: http://www.directvacuum.com/sputter.asp. [Accessed: 23-Mar-2015].

[34] "Mo R100216 - RRUFF Database: Raman, X-ray, Infrared, and Chemistry." [Online]. Available: http://rruff.info/mo/chem=Mo/display=default/R100216. [Accessed: 23-Mar-2015].

[35] L. R. Damiani and R. D. Mansano, "Zinc oxide thin films deposited by magnetron sputtering with various oxygen/argon concentrations," *J. Phys. Conf. Ser.*, vol. 370, p. 012019, Jun. 2012.

[36] A. Blume, "Synthese und strukturelle Untersuchungen Wolframoxiden als Referenzverbindungen für die heterogene Katalyse," 2004.

[37] M. a. Camacho-López, L. Escobar-Alarcón, M. Picquart, R. Arroyo, G. Córdoba, and E. Haro-Poniatowski, "Micro-Raman study of the m-MoO2 to α-MoO3 transformation induced by cw-laser irradiation," *Opt. Mater. (Amst).*, vol. 33, no. 3, pp. 480–484, Jan. 2011.

[38] M. A. Py, P. E. Schmid, and J. T. Vallin, "Raman Scattering and Structural Properties of MoO3," *Nuovo Cim.*, vol. 38, no. 1, 1977.

[39] J. P. Thielemann, G. Weinberg, and C. Hess, "Controlled Synthesis and Characterization of Highly Dispersed Molybdenum Oxide Supported on Silica SBA-15," *ChemCatChem*, vol. 3, no. 11, pp. 1814–1821, Nov. 2011.

[40] a. Hojabri, F. Hajakbari, a. Emami Meibodi, and M. a. Moghri Moazzen, "Influence of Thermal Oxidation Temperatures on the Structural and Morphological Properties of MoO 3 Thin Films," *Acta Phys. Pol. A*, vol. 123, no. 2, pp. 307–308, 2013.

[41] J. Sotrop, M. Domke, a. Kersch, and H. P. Huber, "Simulation of the melting volume in thin molybdenum films as a function of the laser pulse duration," *Phys. Procedia*, vol. 41, pp. 520–523, 2013.

[42] G. Nazri, "Heat-treatment studies of molybdenum oxide-monohydrate," *Solid State Ionics*, vol. 80, no. 3–4, pp. 271–275, 1995.